A study of gold-tin eutectic alloy solidification

AUTHOR:

Martin, Edward Laurence

TITLE:

A Study of Gold-Tin Eutectic Alloy Solidification

DATE: January 16, 1994

A STUDY OF GOLD-TIN EUTECTIC ALLOY SOLIDIFICATION

by

Edward Laurence Martin

A Thesis

Presented to the Graduate and Research Committee

of Lehigh University

in Candidacy for the Degree of

Master of Science

in

Materials Science and Engineering

Lehigh University

1994

Certificate of Approval

This thesis is accepted and approved in partial fulfillment of the requirements for the degree of Master of Science.

December 15, 1993
(Date)

Thesis Advisor

Chairman of Department

I wish to extend my appreciation to my advisor, Dr. M. R. Notis, for his guidance, patience, resourcefulness and support during this study.

Appreciation is extended to SPM Co., Inc. of Marmaroneck, New York for financial support with this study.

Special thanks is given to the following individuals for their contributions without which this thesis would not exist.

Vinay Mishra, for answering many DSC related questions, twice.

George Yasko, for innovation in getting random orientations for XRD analysis.

Arlan Benscoter, for his patience and his expertise in metallography.

Adam Scotch and Kevin Johnson, for their flexibility and their skill in using the Leco image analysis system.

Kathy Repa, for her EM expertise and for always giving a quick liquid N_2 fill-up.

Dr. Richard S. Kontra, for introducing me to Materials Science and Engineering and for being an excellent role model.

My grandmother, Mrs. Mary Kontra, for her sincere interest in my studies, research and success.

I especially thank my family for their financial and emotional support as well as for their total commitment to education. Also, I especially thank Jennifer Chropuvka for being a bright spot to look forward to each day.

I thank the Materials Science and Engineering Department, faculty, staff and graduate students for sharing their knowledge and for their patience. I especially thank Chris Ragazzo and Jason Kosek for their consultation during the creation of this thesis.

It is difficult to say what is impossible, for the dream of yesterday is the hope of today and the reality of tomorrow.

Robert H. Goddard

List of Tables

List of Figures

Abstract

Au-Sn eutectic solder preforms are often used for joining electronic components. The mechanical properties of the joint and the wetting behavior during solidification are closely related to alloy composition. Tight controls on solder alloy composition are therefore normally maintained during manufacturing to insure product quality and reliability. In prior investigations, interpretation of differential scanning calorimetry (DSC), a method used to measure the eutectic melting temperature, has been problematic. Clarification of the alloy melting behavior and its relation to composition is needed. The purpose of this study is to investigate solidification of Au-Sn alloys near the eutectic composition (80 wt.% Au - 20 wt.% Sn) and describe the structure and phase composition using quantitative microscopy and thermal analysis techniques.

In the present study a procedure for quantitative metallography of Au-Sn alloys has been developed which uses a computer program based on Delesse's Principle. Good agreement has been observed between predicted values for both primary phases and eutectic structures. Differential scanning calorimetry (DSC) analysis has been performed on alloys which were studied by quantitative microscopy and a consistent interpretation of the results has been obtained. It is suggested that second heating and cooling cycle results from the DSC measurements be taken as the primary source of analysis and the reasons for this choice are described.

I. Introduction

Au-Sn eutectic alloys are widely used as solders in the microelectronics industry. Superior material properties including high conductivity, high durability, low melting point (280 °C), and low thermal expansion make Au-Sn eutectic solder an excellent material for joining electrical components. In most cases a solder preform is fabricated from cast Au-Sn eutectic alloy by rolling an ingot to a thin sheet and stamping preforms of desired shape out of the thin sheet. The preforms are then placed in joints where soldering is required, and are melted. Ideally, the liquid Au-Sn eutectic alloy wets the surfaces of both components thereby creating a sound electrical and mechanical connection. Device and materials fabricators are very concerned about the reliability of Au-Sn eutectic alloys for this type of solder joining technology. Therefore, suppliers of Au-Sn eutectic alloys are continuously looking for ways to improve the quality and reliability of their product. Additionally, valid, repeatable, and scientifically based testing procedures are needed to identify reliable criteria for manufacturing Au-Sn solder. Because most Au-Sn eutectic solder is used in reflow manufacturing processes it is appropriate to first consider the reflow process.

II. Background

A. *Solder Reflow Process*:

Reflow soldering is a major manufacturing method for joining electronic assemblies. (Figure 1). Opportunities exist for assemblies with components on both sides of a printed circuit board and assemblies which contain a mixture of surface mount and through-hole components. The dynamics of the reflow process must be properly understood. The most important processing factors include [1]:

Melting behavior and related properties of the molten solder
Reflow time-temperature profile
Metallurgy of surfaces being joined

Dynamics Of Solder Reflow Process

Au-Sn solder preforms have recently been utilized in new, high reliability reflow processing techniques. For example in fluxless and virtually voidless soldering of semiconductor chips. "It is essential for the process to use a washer preform instead of a square [2]". Another example involves the use of Au-Sn solder preforms in multilayer bonding process [3].

B. *Wetting:*

Solder alloys have two primary functions. First, solder alloys mechanically bond together the various members of an electrical connection. Second, solder alloys conduct

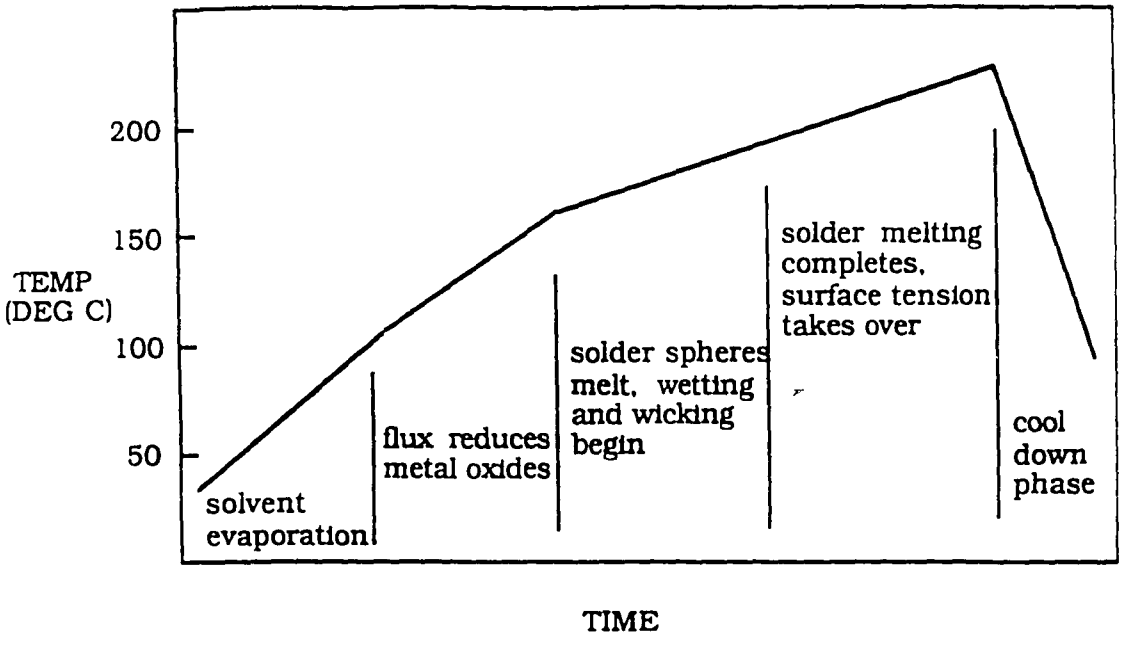

FIGURE 1: Solder Reflow Sequence [1]

electricity between members of an electrical connection. Solders also conduct heat away from temperature sensitive microchips. Wetting behavior is the most important physical attribute of a solder connection. The most important visible attribute of a solder joint is the shape of the fillet. If the fillet shape is concave (curves away from your eye) this indicates good wetting. Poor wetting, with some exceptions, is indicated by a convex (curves towards your eye) fillet [4]. Wetting is described by a liquid droplet resting on a flat horizontal surface. Wetting occurs when $\Theta < 90^{\circ}$ (Figure 2a). Non-wetting occurs when $\Theta > 90^{\circ}$ (Figure 2b) [5].

Two factors influence whether or not a solder will wet a connection. First, the surfaces of the connection must be hot enough so that the solder does not freeze upon contact. The higher the surface temperatures are above the melting point of the solder, the quicker wetting will occur. Second, molten solder does not normally wet oxides. Most metals react with oxygen to form surface metal oxide films. These oxides must be removed, usually by a flux, before wetting can occur [4].

C. Au-Sn Solders:

The most recent phase diagram for the Au-Sn system [6] is shown in Figure 3. The most commonly used solder alloy is of the eutectic composition (29.0 at.% Sn = 19.75 wt.% Sn). This eutectic melts at 280 °C and when solid, consists of two phases: δ phase (AuSn: 50 at.% Sn = 37.6 wt.% Sn) and ζ phase (17.6 at.% Sn = 11.4 wt.% Sn). There is a peritectoid reaction at 190 °C where the ζ phase transforms to ζ' phase (Au_5Sn: 16.7 at.% Sn = 10.4 wt.% Sn). The normal criteria used for quality control compliance for the

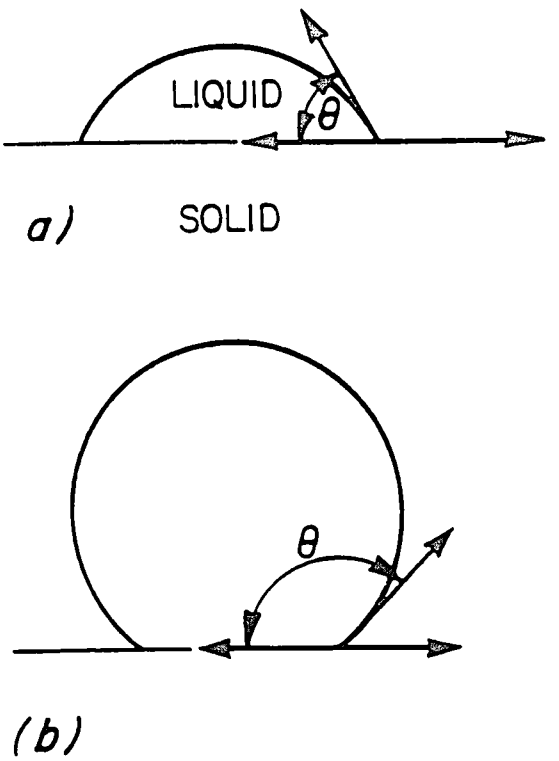

FIGURE 2: Equilibrium configuration of a liquid droplet on a solid substrate for conditions of (a) wetting, and (b) nonwetting [5]

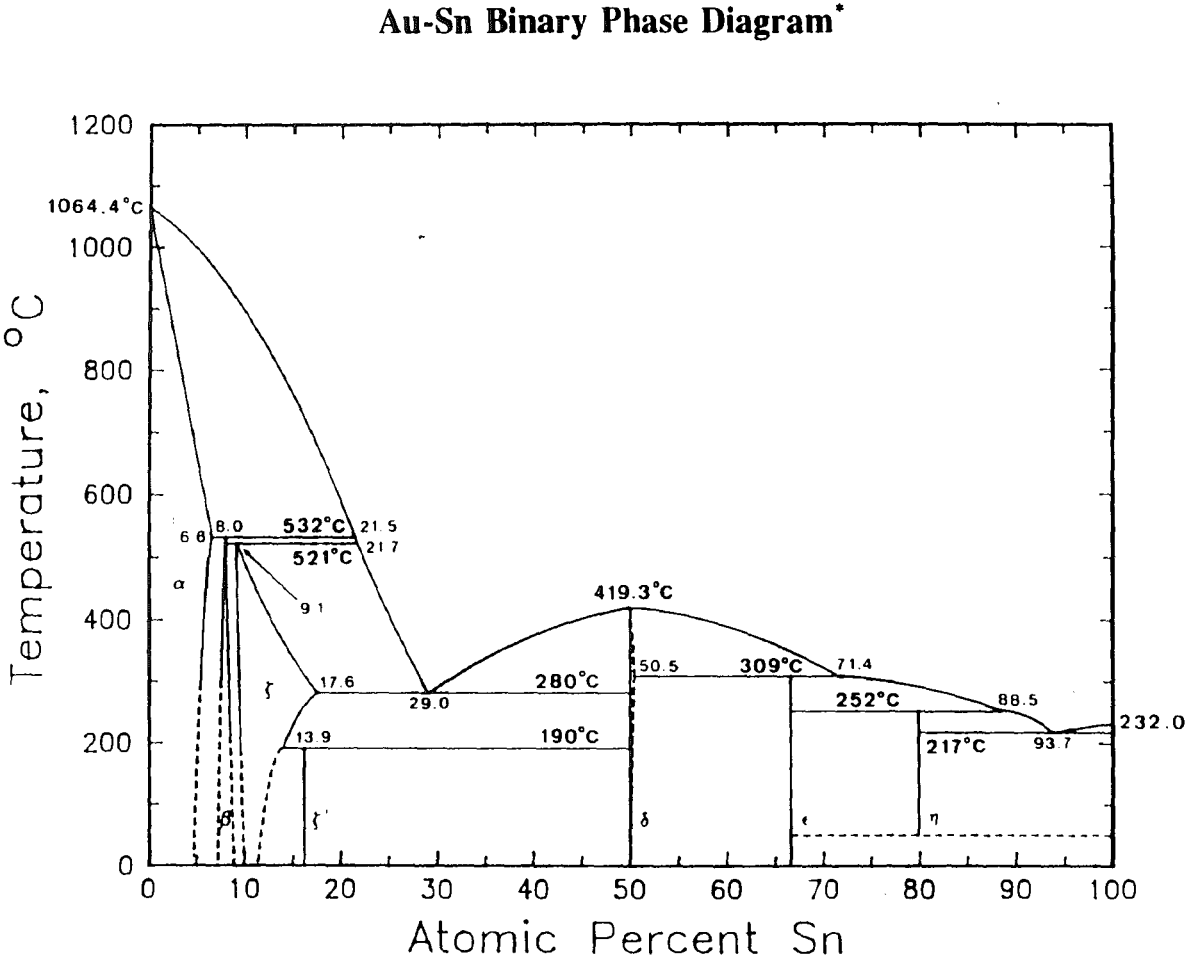

FIGURE 3: Au-Sn Phase Diagram [6]

eutectic solder is a chemical analysis to check for impurities, and a thermal analysis to check for the melting temperature of the eutectic (commonly taken as 280 °C ±1 °C).

In the recent literature, Johnson and Wolverton [7] point out a reliability concern regarding the consistency of Au-Sn eutectic solder. A blistering problem was encountered when using Au-Sn eutectic solder in a reflow application. These blisters could lead to a weakened mechanical joint, a poor electrical connection and could have potentially allowed loose chips of metal to flake away from the joint and cause shorts elsewhere within the electronic device. The source of the blisters was attributed to the presence of intermetallic particles which were believed to be retained from a prior Au-Sn intermetallic phase, epsilon (ε). It was hypothesized that these hard, higher-melting-point particles or regions failed to melt at the reflow temperature. Because some solder areas failed to melt, regions of non wetting were created on the surfaces in the joint. When the liquid metal was caused to cool around the non-wet area, it stressed, weakened, cracked and caused blistering [7].

Other users have also experienced voids which caused inferior solder joints. Wassink [8] points out that voids which form during soldering are due to shrinkage during solidification and are eliminated usually only by vacuum degassing during the solidification process. Mizuishi, et. al., [2] using a 40 wt.% Pb - Sn solder, have used this vacuum degassing approach to produce fluxless and nearly-void-free solder joints. Mohanty [9] has provided a theoretical basis for the explanation of this phenomena in terms of heterogenous nucleation of pores during the solidification process. In the specific case of Au-Sn solders, Lee, et. al.,[10] have shown that voids are eliminated by

using a vacuum cycle and Nishiguchi, et. al.,[11] have shown similar results using an applied load (pressure) during joining.

In the previously referred to paper by Johnson and Wolverton [7], differential scanning calorimetry (DSC) curves for the offending solders were noted to often contain a suspicious, additional peak at a temperature greater than the melting point of the solder. This DSC peak appeared as a broad shoulder attached to the main melting peak. X-Ray Diffraction (XRD) analysis also indicated x-ray intensity peaks which were attributed to trace amounts of Au-Sn intermetallic epsilon (ε) phase. The two observations were linked by the investigators.

D. Purpose of Study:

The interpretation suggested by Johnson and Wolverton [9] was that the results of the thermal analysis could be correlated with the results of wetting or bonding tests. The present study, as outlined below, was initiated because of questions concerning the proper interpretation of thermal analysis methods as related to eutectic or near-eutectic structures, and how these relate to alloy composition and microstructure. Therefore, the purpose of this study is to describe the Au-Sn eutectic solder manufacturing process, to examine microstructure and obtain thermal analysis of alloys at or near the eutectic composition and to refine the criteria for determining what is an acceptable solder alloy for manufacturing purposes. The format for the experimental approach will be as follows:

1.) Comparison of traditional casting and continuous casting.

2.) DSC evaluation. Significance of DSC plots.

3.) XRD consideration.

4.) Quantitative metallographic analysis:
Wt. % → Area % in microstructure
calculations (via computer), and vice versa.

Experimental Summary

III. Experimental Procedure

A. *Alloy Fabrication:*

Three different Au-Sn alloy manufacturing methods were used in this study. The first and most simple method was to melt together small quantities of gold and tin and these were fabricated in the laboratories at Lehigh University. For these as well as the other alloys, Au and Sn starting materials had purities of 99.99% or better. The component metals were weighed out, placed in a test tube, submerged in glycerine or a high purity oil with a higher boiling point than that of glycerine, and melted over a Bunsen burner. The test tube used was Pyrex with dimensions of (O.D. = 10mm, L = 75mm). Tin melted first, wet the surface of the gold, then alloyed with the gold. The test tube was swirled by hand during melting to promote mixing and the tube was then allowed to cool in air. The small size of the test tube allowed solidification to occur within a few seconds; the specimen was cool enough to handle within a few minutes. The solidified pellet (weight ~ 250 mg) was easily removed from the test tube and had a fairly bright surface appearance.

The second alloy fabrication method, performed by a commercial manufacturer, used a conventional casting procedure in which the following steps were followed:

1.) Heat pure Au to between ~648 - 815 °C
2.) Insert scrap (being careful to keep alloy Au-rich at all times)
3.) Add pure Sn after prior melt appears homogeneous
4.) Heat to ~871 °C then cool to ~427 °C
5.) Evacuate in vacuum chamber (20-50 microns), for 5 min.
6.) Heat again to below red heat and skim slag & oxides from surface
7.) Pour into a preheated (~315 °C) mold
8.) Skim off surface residues
9.) Air cool under protective cover

Conventional Casting Procedure

A high frequency induction furnace was used with (N_2 (85%) - H_2 (15%)) gas blown over the surface of the melt to prevent oxidation. The crucible was made of clay-graphite and the mold was made of high purity graphite. The mold size allowed an ingot of approximate size 16" X ½" X 2½" to be cast (weight ~ 150-160 oz.), and typically the ingot could be removed from the ingot after fifteen minutes (Figure 4).

The third alloy fabrication method, used by the same manufacturer, was to use a continuous caster (Figure 5). Pure Au, pure Sn and scrap were alloyed together under a vacuum. Two 100 oz. ingots of Au-Sn eutectic were cast and were then charged into the continuous caster at the same time. The continuous furnace was manufactured by Rautomeade, model RMJ/H005. The ingot width and height on exit from the furnace are 3½" X 0.098", the length of the ingot is variable, depending on how long the job runs. The ingot step rate is 3"/min with a ⅛" pulse. N_2 is the gas atmosphere in the furnace.

B. Differential Scanning Calorimetry (DSC):

Differential Scanning Calorimetry (DSC) detects thermal events which evolve or

a

b

FIGURE 4: Vendor 'X' Traditional Casting Procedure
a.) Raw Materials b.) Melting

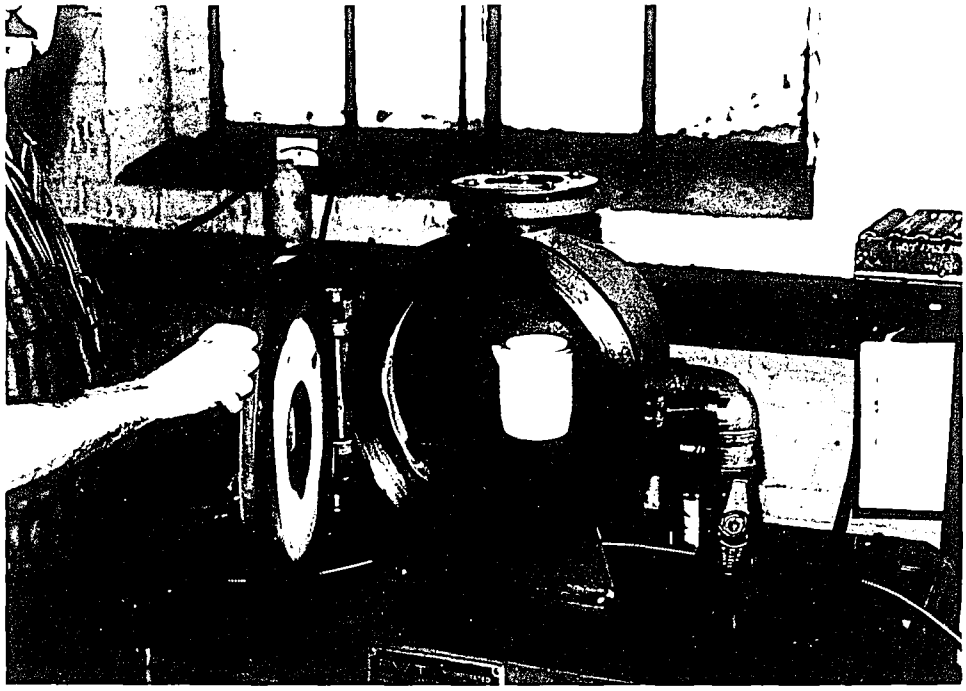

c

d

FIGURE 4: Vendor 'X' Traditional Casting Procedure
c.) Vacuum Degassing d.) Pouring

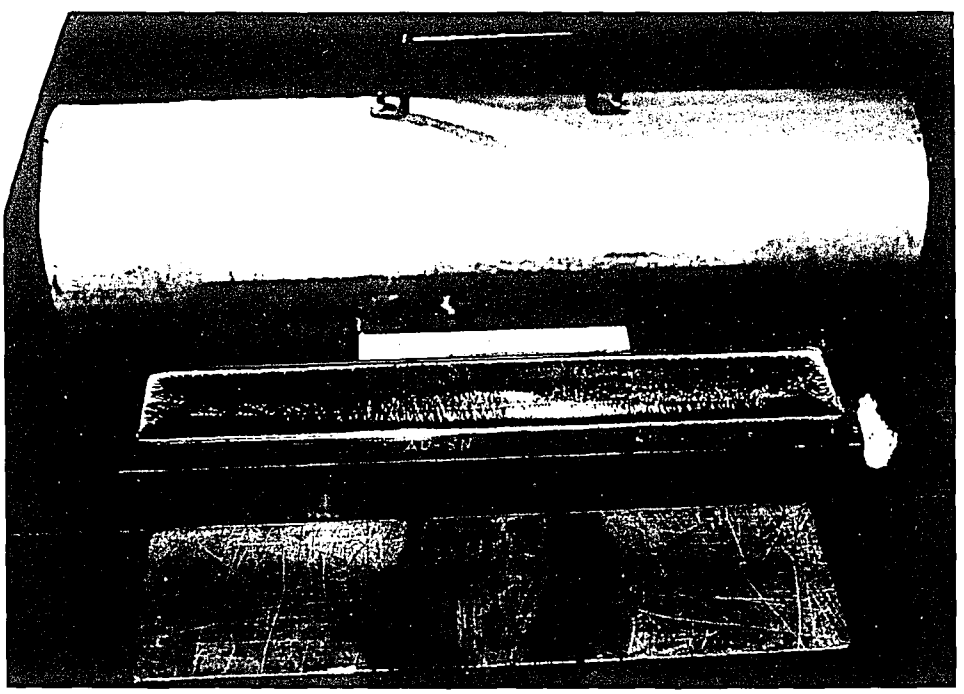

e

FIGURE 4: Vendor 'X' Traditional Casting Procedure
e.) Cast Ingot

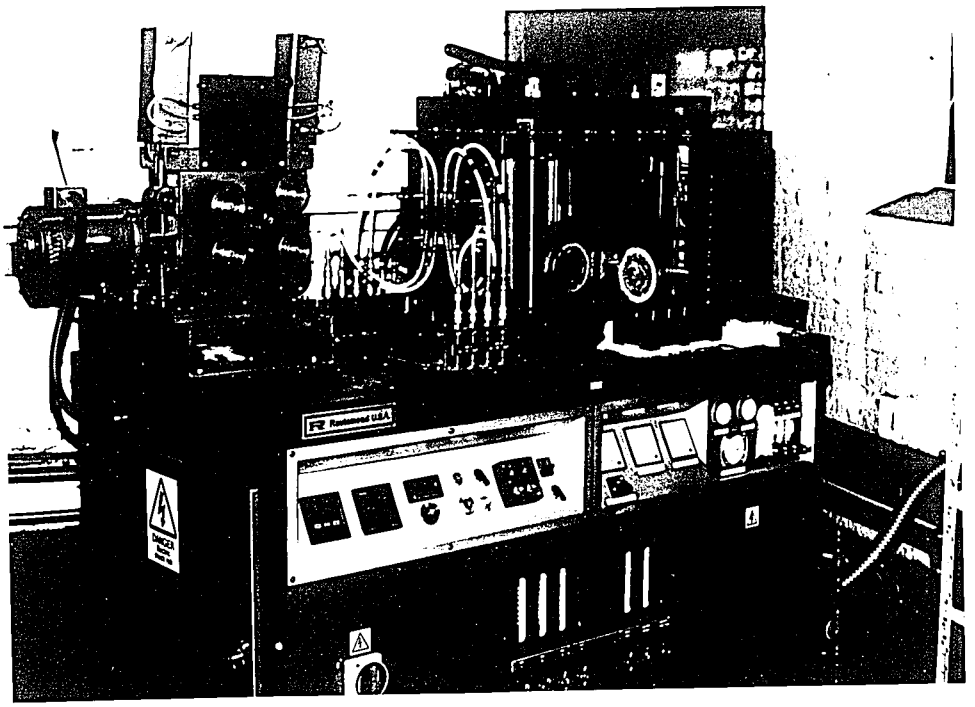

a

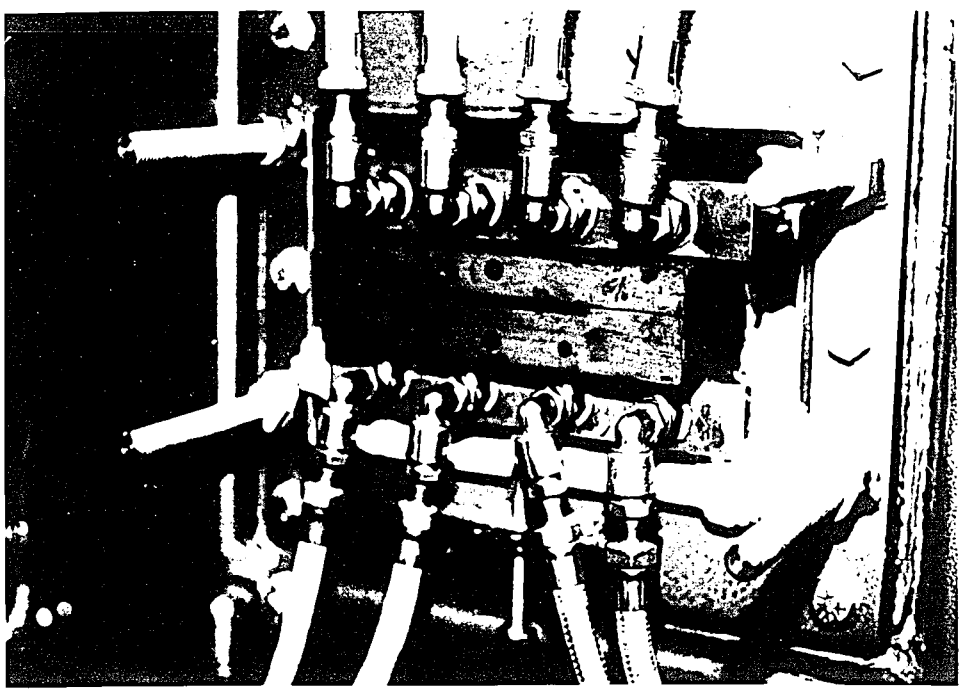

b

FIGURE 5: Vendor 'X' Continuous Casting Equipment
a.) Continuous Caster b.) Exit Chamber

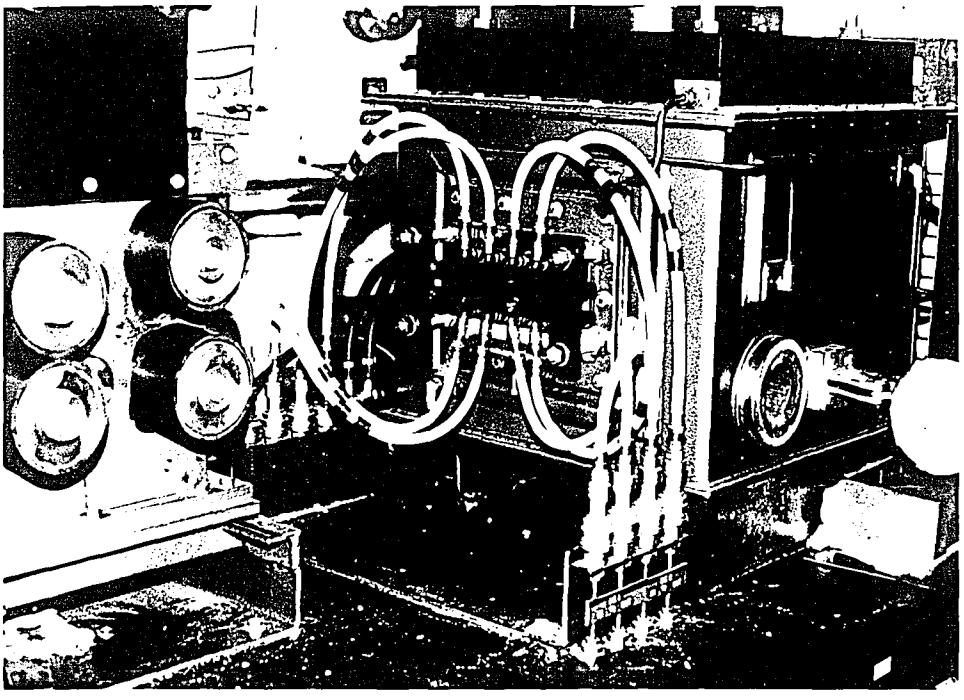

c

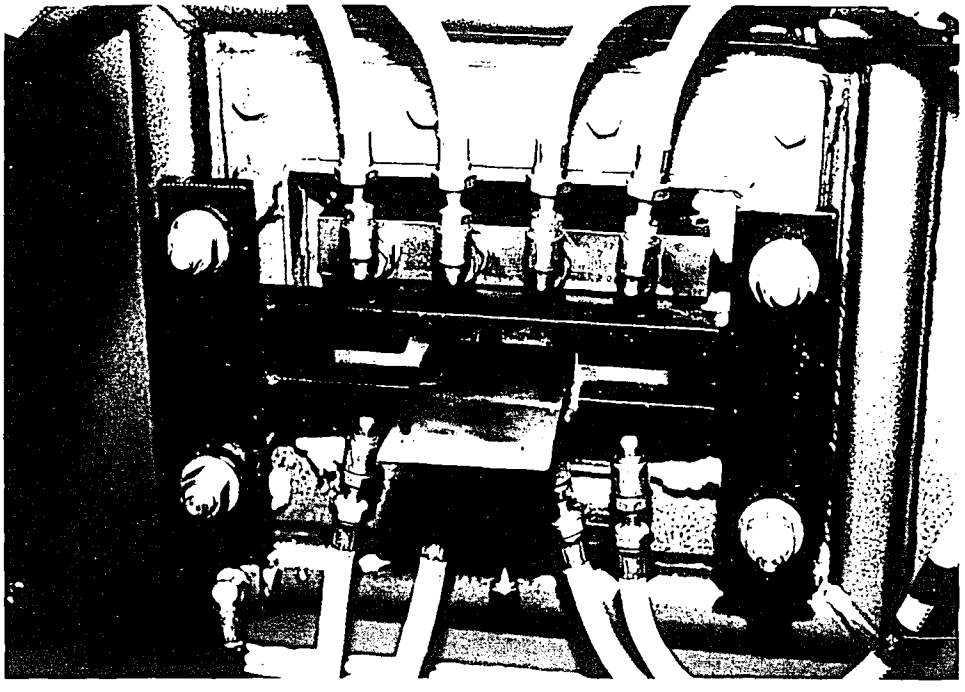

d

FIGURE 5: Vendor 'X' Continuous Casting Equipment
c.) End View d.) Starter Bar Protruding from Mold

absorb heat as a function of temperature [12]. For example, as ice is heated from below 0°C to above 0°C it melts, and melting is an endothermal thermal event which can be detected using DSC.

During a DSC scan, the sample of interest and a reference sample are placed in the same chamber and exposed to identical temperatures and atmospheres at exactly the same time (Figure 6). Within the chamber are independent thermometers which simultaneously measure the temperature of both the sample and the reference. There are also independent heating elements for both the sample and the reference. A heating (cooling) rate is programmed into the DSC's computer and an electronic controller keeps the sample and reference at the exact same programmed temperature even though the sample may experience an internally generated thermal event. The amount of energy which must be supplied to or withdrawn from the sample to maintain a zero temperature differential between the sample and the reference is plotted as a function of temperature (Figure 7) [12].

The rate at which a sample absorbs or emits energy is proportional to the specific heat of that sample. Transitions accompanied by large changes in specific heat produce signal discontinuities. Exothermic or endothermic enthalpy changes yield peaks whose areas are proportional to the total enthalpy change.

Temperature ranges of DSC instruments vary based on the variety of materials being tested. The DSC instrument used in this study (Mettler TA3000) is in fact equipped with a low temperature cell and is generally used for polymer studies. However, because all Au-Sn alloy thermal transitions of interest here are expected to occur below $T \approx 450\,°C$,

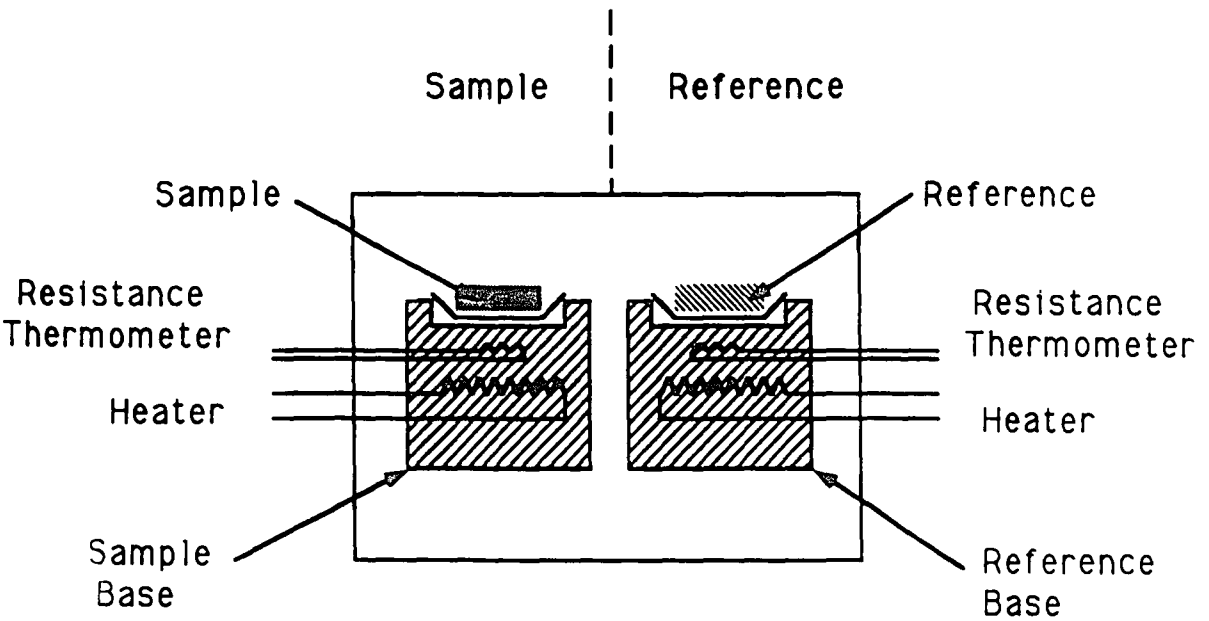

FIGURE 6: Schematic diagram of the DSC Measuring Cell [12]

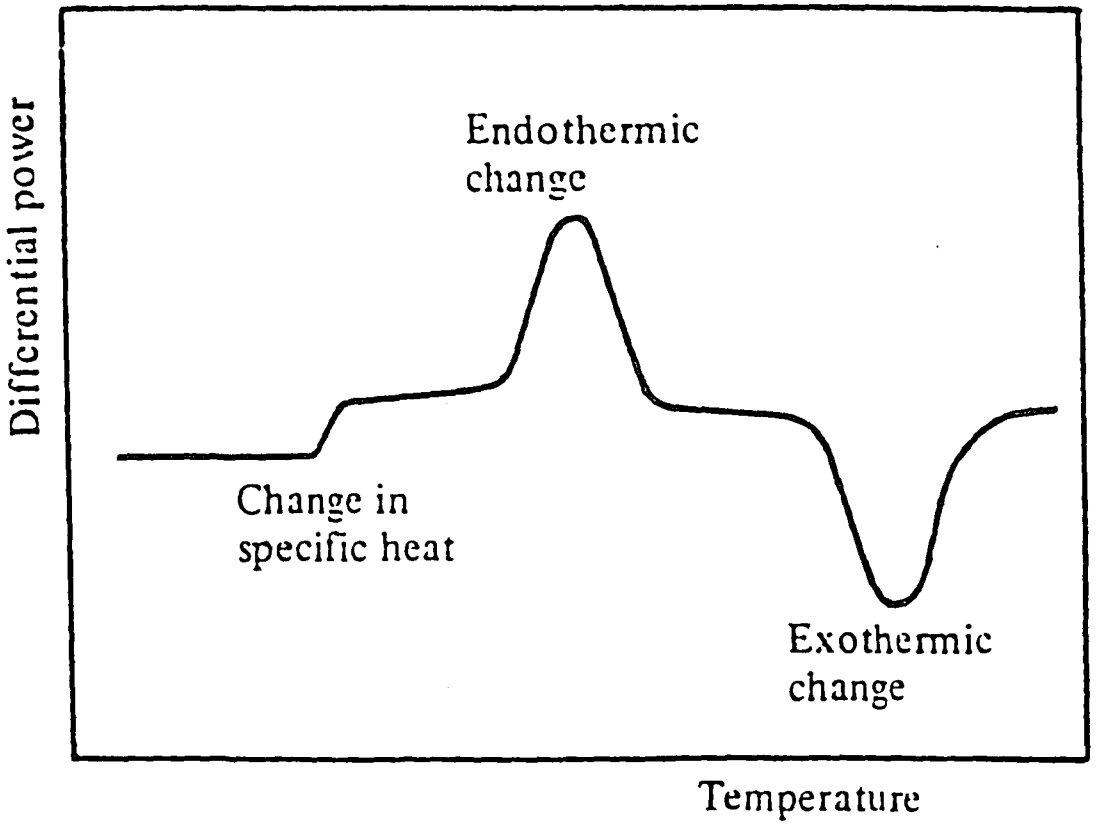

FIGURE 7: Schematic of a typical DSC Trace [12]

this unit worked well. Aluminum pans were used to hold the samples and the reference because $T_m(Al) = 660°C$; this is much greater than any transition temperature expected in alloys tested and is also well above the heating capability of this DSC unit equipped with a low temperature cell.

Temperature is measured by platinum resistance thermometers. The resistance of platinum has a well known relation to temperature and by comparison to the melting points of known elements in the DSC cell, a polynomial fit can be applied to the non-linear temperature dependence:

$$R(T)=A+BT+CT^2$$

where A, B, and C are determined by calibration. For calibration of the DSC instrument used in this study, A = 156.6, B = 327.4, C = 419.5 corresponding to the fusion points of In, Pb and Zn [12]. The measurement cell measures heat output sent to both the sample and the standard to keep them both at the program temperature. A microprocessor automatically calculates reaction temperatures based on the difference in heat supplied to each. A temperature lag is inherent in all DSC equipment meaning that the actual furnace temperature lags behind program temperature. This effect is automatically compensated for by the DSC electronic controller. The error, ΔT, associated with DSC data can be expressed by the following equation:

$$\Delta T=2S\left(\frac{T-T_2}{(T_3-T_1)/2}\right)^2$$

where T is the measured temperature of transition, T_1, T_2, and T_3 are the lower, middle and upper calibration temperatures and S is the precision of the measurement obtained from the testing of known samples. (S is the thermometric sensitivity of the DSC sensor and is given by the number of points per °K. For the DSC unit used in this study S = 2400) [12].

The melting temperature is obtained from a DSC curve by locating the largest peak which is near the known melting point. Other, smaller peaks also correspond to transformations, but the melting peak should be the largest. The melting point is located at the position where the curve first begins to rise, *not at the peak of the curve.* There are several methods to determine this point automatically; they involve curve fitting techniques such as plotting tangents to the peak and to the baseline curves and computing the intersection point. Therefore different definitions of onset points can be used and slightly different values of (T_{mp}) determined using these methods, depending on which default values are chosen. The onset temperature is usually best chosen by drawing a line from where the peak 'takes off' to its intersection with the local baseline.

In this study, DSC samples were cycled through the following heating and cooling rate range: heat at 10° C / min., cool at 100° C / min., heat at 10° C / min., cool at 100° C / min.(except where noted). When DSC curves are presented in this study, *only the second heating and second cooling curves will be shown* (except where noted); they generally display the most consistent data with the least extraneous fluctuations. This procedure is in good agreement with previous work reported on Pb-Sn alloys where it was found that the second cycle allowed good thermal contact with the pan and also removed

the inhomogeneities present in the alloys [13]. Typically, repeated measurements on the same sample are repeatable to ±0.2 °C. For example, the melting point of pure Pb could be determined to be consistently repeatable to this level of measurement.

C. X-Ray Diffraction (XRD):

X-Ray Diffraction (XRD) can be used to detect and identify different phases which may be present in a multi-phase alloy. In this method an X-ray beam bombards the sample and is diffracted at different angles. Diffraction peaks exist at certain diffraction angles for each phase which is present. In this method an X-ray beam bombards the sample and is diffracted at specific angles. If the spacing of the atomic planes causing diffractions satisfies the Bragg equation:

$$n\lambda = 2d\sin\Theta$$

(where n is instrumentally selected to be 1, λ is wavelength of monochromatic X-rays, d is the interplanar atomic spacing, Θ is the Bragg angle), then the reflected waves will interfere constructively and a peak will be observed [14]. The relative height of the peak will be proportional to the amount of phase giving rise to the peak. For each phase there are a number (usually taken as three) of interplanar atomic spacings which produce Bragg diffraction conditions. One of these interplanar spacings is usually the strongest intensity peak. The other two interplanar spacings are less intense relative to the primary interplanar spacing but are used to confirm the presence of a particular phase (the presence of these two supplemental atomic spacings confirms the presence of a given phase, but their absence does not necessarily indicate the absence of that phase). In this

study if a DSC sample was found to exhibit an unexpected shoulder or an unexpected additional thermal peak, the specific sample was tested using X-ray diffraction. Typically, only the (δ) phase and (ζ') phase were both confirmed, with many counts at nearly all of the characteristic interplanar spacings expected for those two intermetallic phases. Other peaks were also sometimes visible in the spectrum; however, these were smaller peaks and could not reliably and consistently be attributed to any other Au-Sn intermediate phase or to any known contaminant.

D. Metallographic Preparation:

Each sample was sectioned using an Isomet slow-speed diamond saw. Samples were mounted in Leco epoxy, placed under vacuum for several minutes and cured overnight at room temperature. The samples were then ground in kerosene using 320, 400 and 600 grit SiC grinding paper with a lubricant of paraffin. This lubricant reduced SiC particles becoming embedded in the soft gold-rich phases. Grinding continued through 8 and 3 μm SiC grinding paper with the same paraffin in kerosene lubricant. Polishing with 1 μm diamond paste followed grinding. Final polishing was performed using colloidal silica in a Buehler automatic vibratory polishing machine. Etching was accomplished with aqua regia in one of two concentrations depending on the specimen response. The following mixtures are the specific compositions used:

Dilute:	(40% HCl - 10%HNO_3 - 50% H_2O)
Concentrate:	(33.3% HCl - 33.3% HNO_3 - 33.3% H_2O)

Aqua Regia Etching Concentrations

Various etching times were used. Usually, thirty second intervals were chosen until satisfactory delineation of the phases was achieved [15]. Smeared metal presented a great challenge during final polishing and etching. Many etch-polish-etch cycles were needed to remove all the smeared metal which accumulated from grinding. An intermediate stage exists (Figure 8) where numerous circular regions of smeared metal have been removed and etched, but most of the surface is still smeared and presents a false microstructure.

Overetching caused surface cracks in the microstructure along the boundary between the (δ) phase and (ζ') phase lamellae (Figure 9). This phenomena is still being investigated.

E. Digital Image Analysis:

After samples were polished and etched, area percentages of each phase present were measured using a Leco digital, computerized image analyzer. This approach is chosen for a number of important reasons. First, because a computerized image analysis process may be obtained, optimized and saved for many images. Second, because once optimized, the image analysis process emphasizes computer processing and minimizes

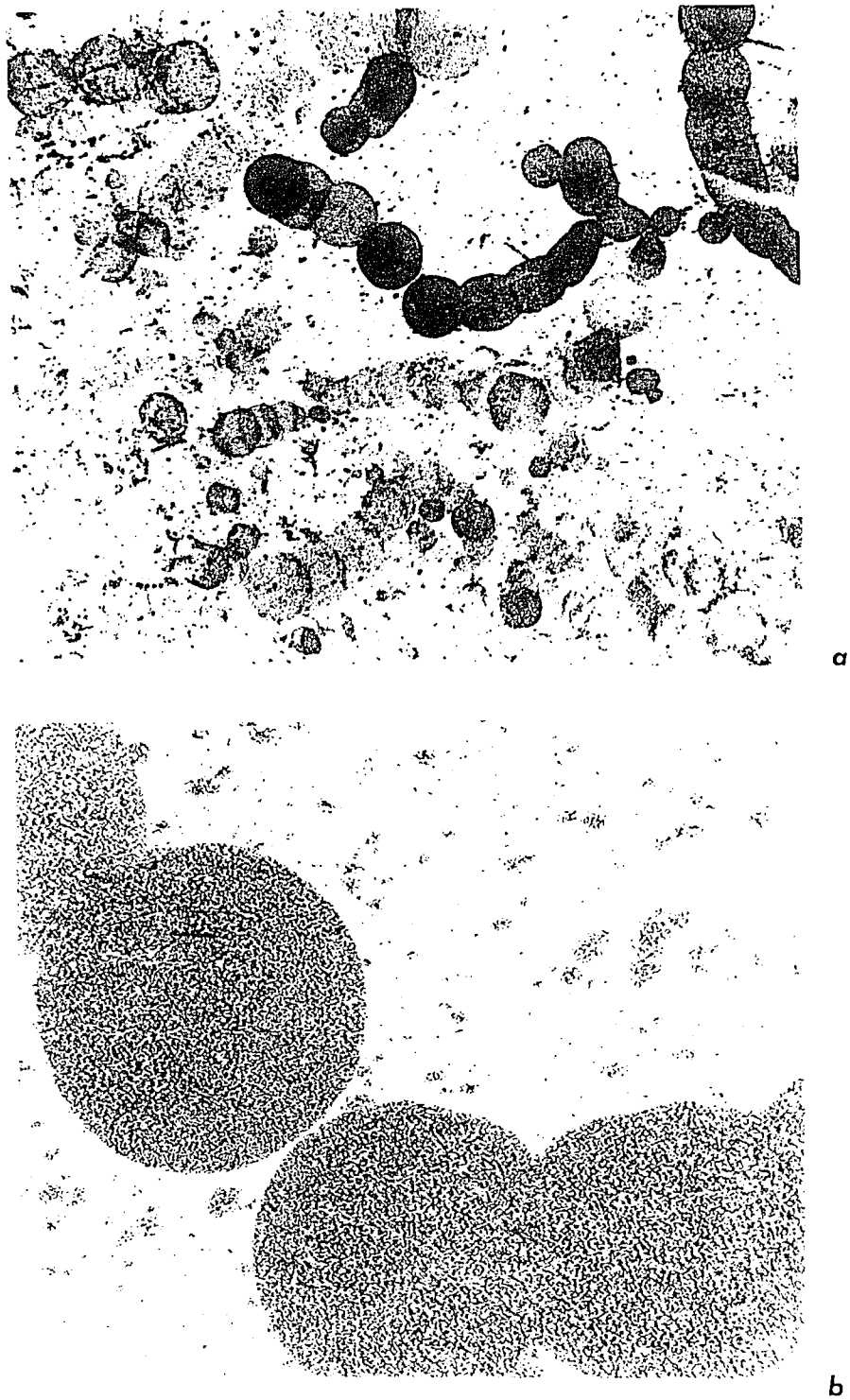

FIGURE 8: Polishing Defect. Spherical areas are etched, remaining area is not. Optical Microscopy a.) 50X b.) 250X

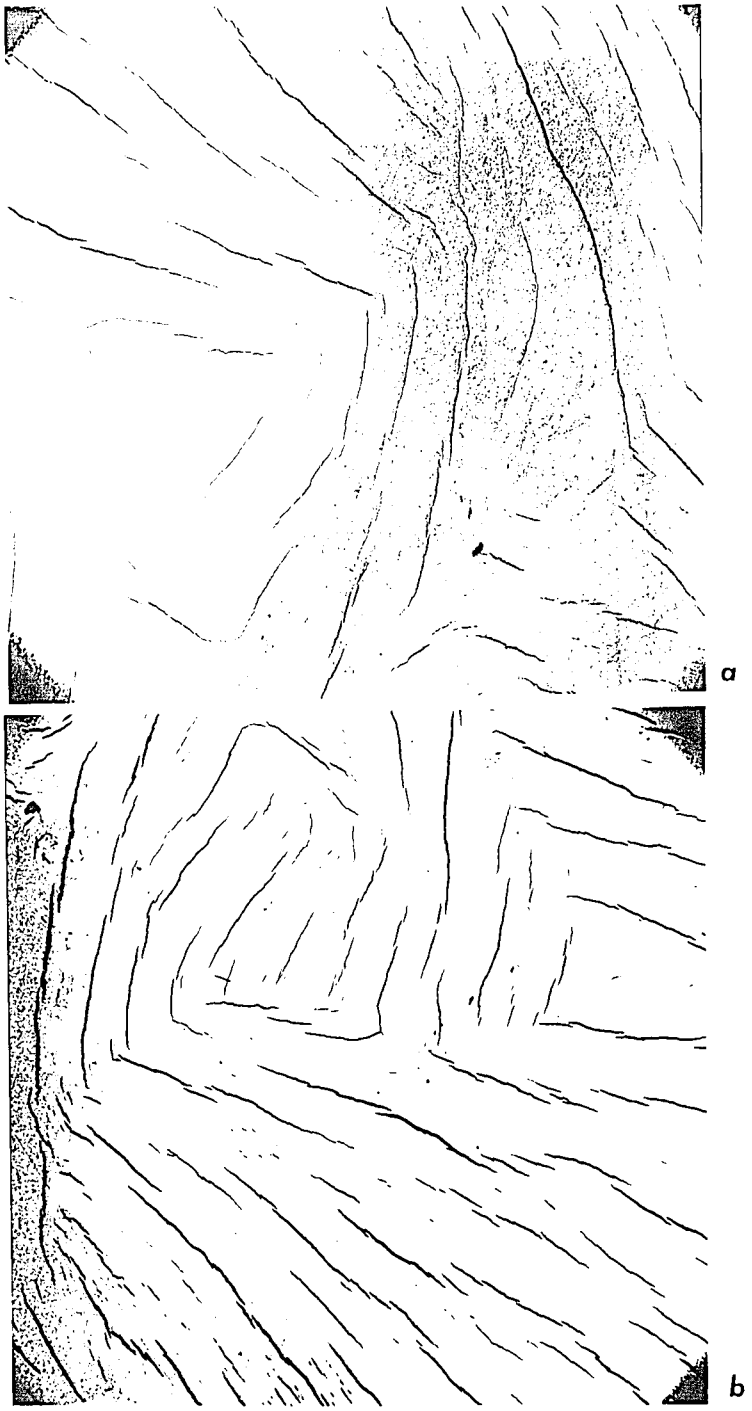

FIGURE 9: Etching Defect. When a sample is overetched cracks appear along the boundaries between the (δ) and (ζ') phases. However, at the same time the surface is still covered by smeared metal, therefore, the microstructure is not visible, but the cracks are visible.

a.) SEM Secondary Electron Collection Mode (300X) [16]
b.) SEM Backscatter Electron Collection Mode (300X) [16]

user input and user bias. Thus, image analysis via computer is repeatable so that results are statistically sound.

Images are 'read in' to the computer through a closed circuit black and white video camera which is directly attached to a microscope on which the sample sits. A live, digital image is obtained (Figure 10a) and stored on screen for analysis. First, the dimensions of a primary microstructural feature are recorded. The image is then optimized, sharpened,and calibrated using pre-programmed software functions. Care is taken to preserve the original dimensions of the microstructural feature that was selected. During the optimization process contrast is optimized so that the entire graphic capability of the instrument is utilized. This means that nearly 100% of the pixels in the image have some gray level between 100% black and 100% white, while very few pixels are actually 100% black or 100% white. Each digital image which is presented in this study will have a graph showing how many pixels of each gray level are in that image, the graph is called a *histogram* (Figure 10b). Beneath the histogram there will always be a bar graph showing which gray levels the computer is choosing to analyze (Figure 10b). The gray levels which are chosen by the computer for analysis are highlighted red in the image (Figure 10b).

After a microstructural feature is highlighted, a comparison of the red dimensions to the original dimensions is made, in order to insure that a net change in measured area did not occur during the image optimization and area selection process.

Generally, measurements of area fractions are recorded until a consistent value is obtained. Every time a microstructural area measurement is presented in this study it will

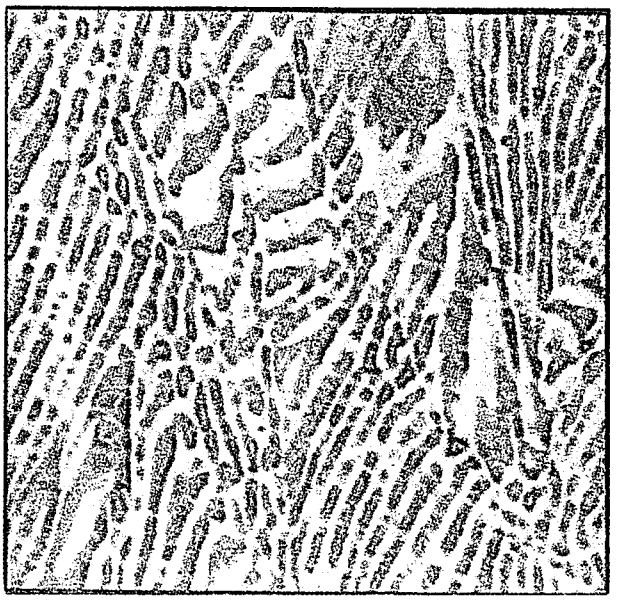

a

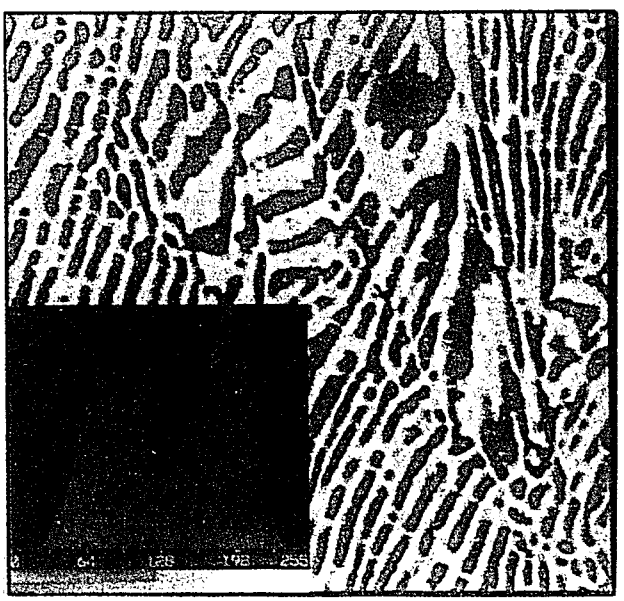

b

FIGURE 10: a.) Digital computer image of Alloy "E" (80.87 wt.% Au - 19.13 wt.% Sn) (2000X).

b.) Microstructure area percentage selected for analysis by the computer (2000X).

have a 1σ value presented along with it to indicate the reliability of the value being presented [17, 18, 19, 20]. Typically, about twelve measurements were made on each sample studied, after consistent operation was established.

IV. Calculations

Mechanical properties of materials are dictated by their microstructures and the phase properties of which they are comprised. In the case of an eutectic alloy, the volume percent of each phase and its' morphological distribution, is very important in determining the mechanical behavior of the solder alloy. Examination of the Au-Sn phase diagram indicates that, *at room temperature*, the composition corresponding to the eutectic alloy is expected to consist of the zeta prime (ζ') phase (Au_5Sn) and the delta (δ) phase (AuSn).

In conjunction with the calculations from quantitative metallography, for the sake of simplicity, the Au-rich phase was always taken as ζ' (16.07 at.% Sn = 10.4 wt.% Sn) because this is the equilibrium phase at low temperature and it has constant composition, and the 190 °C peritectoid transformation peak was usually observed in DSC plots. X-ray diffraction results are also consistent with (ζ') + (δ) Ciulik [15] indicates that gold-tin alloys heat treated at 170 °C consist entirely of (ζ') + (δ). (ζ') and (δ) are also line compounds whose densities are well defined. The eutectic composition was taken as 20 wt.% Sn, close to both the equilibrium value from the various phase diagrams and the nominal composition of the standard commercial eutectic alloy.

The amount of each phase present is predicted by using the reverse lever rule and tie lines [21]. This approach predicts the relative amounts by weight of each phase (Figure 11).

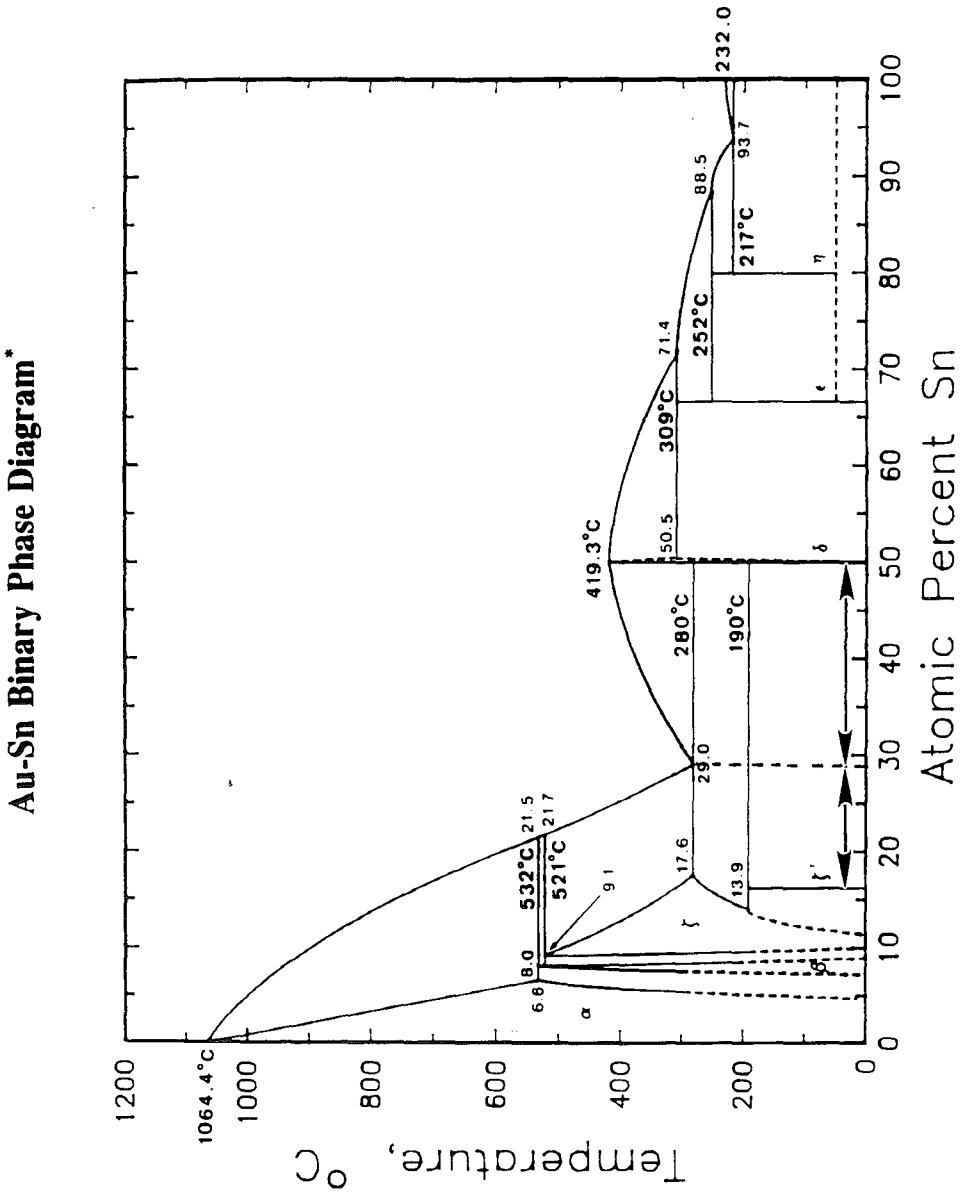

FIGURE 11: Au-Sn Phase Diagram [6] with tie lines shown

wt.% (ζ') phase = {(37.6 - 20) / (37.6 - 10.4)} • 100 = 64.7 wt.%

wt.% (δ) phase = {(20 - 10.4) / (37.6 - 10.4)} • 100 = 35.3 wt.%

Phase Weight Percentages Predicted by Tie-Lines and Reverse Lever Rule

This calculation predicts that the microstructure of an 80 wt.% Au - 20 wt.% Sn eutectic alloy would consist of 64.7% (ζ') phase and 35.3% (δ) phase by weight. However, this calculation does not predict the quantity of each phase that should be observed in the microstructure, which would be in *area percent* or *area fraction.*

The quantitative basis for stereology is now firmly established. The majority of this work relates to image analysis and quantification which demonstrates the equivalency of point counting and area measurement methods and which show that:

$$N_N = L_L = A_A = V_V$$

i.e., that the number of random points in a phase, equals the number of random line lengths crossed, equals the area fraction of the phase, and these equal the volume percent of the phase examined in a given microscope area.

Much less clearly defined is the relationship between volume fraction and weight fraction. The last is significant because it is through this relationship that microstructures can be related to phase diagrams.

The first attempt at such a relationship was made in 1848 by Delesse [22, 23], who proposed that a relationship exists between weight percent and area percent as follows:

$$P_1 = S_1 \bullet (d_1 / d_2)$$

S_1 = % area of phase 1
P_1 = wt. % phase 1
d_1= density of phase 1
d_2 = density of phase 2 (matrix)

Delesse's Principle

A similar but more rigorous approach to that taken by Delesse may be outlined as follows. If the volume (V) of a phase (cm^3) is expressed in terms of its weight (W, grams) and density (ρ, grams/cm^3) then:

V_1 = Volume Portion of Phase 1 = (W_1 / ρ_1)

V_2 = Volume Portion of Phase 2 = (W_2 / ρ_2)

$V_T = V_1 + V_2$

Volume Portion of Phases

The weight fraction of phase 1 would be given as:

$$W^f_1 = W_1 / (W_1 + W_2)$$

$$W^f_1 = (V_1 \bullet \rho_1) / \{(V_1 \bullet \rho_1) + (V_2 \bullet \rho_2)\}$$

Weight Fraction of Phase 1

Multiplying by 100 (to convert to percent), and dividing the numerator and denominator by V_T, gives:

$$W_1\% = (V_1 / V_T \bullet \rho_1) / \{(V_1 / V_T \bullet \rho_1) + (V_2 / V_T \bullet \rho_2)\} \bullet 100$$

Equation 1: Weight Percent of Phase 1

where (V_1 / V_T) and (V_2 / V_T) are the appropriate volume fractions. This equation is the same as equation (11) of Z. Paley and W. M. Willliams [24].

For the case of a small area fraction of a second phase, i.e., a small percent of slag particles in a metallic iron matrix, as was the case of Delesse's work, if the weight fraction of phase 1 is small, then $(\rho_1 \bullet V_1) << (\rho_2 \bullet V_2)$ and,

$$W_1\% \cong \{(\rho_1 \bullet V_1) / (\rho_2 \bullet V_2)\} \bullet 100$$

Further, if the weight fraction of phase 1 is small, then the weight fraction of phase 2 (i.e., matrix) must be nearly equal to the total weight fraction $(V_2 \sim V_T)$ and,

$$W_1\% = \{(V_1 / V_T) \bullet (\rho_1 / \rho_2)\} \bullet 100$$

which is the same as Delesse's Principle!

Equation (1) may be used for the conversion of weight to area fraction of eutectic or off-eutectic alloys. For a simple eutectic, the volume portions, weight percents and densities refer to these values for the end member solid solution phases. For a eutectic whose phases consist of intermediate phases, the same above relationships would hold except that the values for phase densities would be those of the intermediate phases.

For the 80 wt.% Au - 20 wt.% Sn eutectic alloy under consideration, the reverse lever rule gave 64.7 weight percent (ζ') phase. The density of (δ) - AuSn is 11.74 g/cm^3 and the density of (ζ') - Au_5Sn phase is 17.08 g/cm^3. Using Equation (1) and solving for the volume (area) percent $(V_{\zeta'} / V_T)$ gives 55.8 % (ζ'); the expected volume (area) percent

of (δ) phase would therefore be 100 - 55.8 = 44.2 %.

A similar calculation can be carried out for the volume (area) percent of the primary phase on either side of the eutectic composition. For an alloy of composition 80.87 wt.% Au, (19.13 wt.% Sn), the weight percent primary (ζ') phase and wt.% eutectic would be:

wt.% (ζ') ={(20 - 19.13) / (20 - 10.4)}• 100 = 9.1 wt.%

wt.% (eutectic) = {(19.13 - 10.4) / (20 - 10.4)} • 100 = 90.9 wt.%

Wt.% primary (ζ') phase and wt.% (eut.) in an 80.87 wt.% Au alloy

It would be convenient, for the purpose of calculation, to consider the eutectic as a "phase" in order to be able to use Equation (1) to convert the weight percent (ζ') primary phase to volume (area) percent. If we assume 100 g total of "eutectic phase" then the "density" of the eutectic "phase" would be:

Assume 100 g total eutectic phase
ρ = density (g/cm^3)

Total volume of eutectic = $(100 \bullet \text{wt.\%}(\delta) / \rho_{(\delta)}) + (100 \bullet \text{wt.\%}(\zeta') / \rho_{(\zeta')})$

wt.% (δ) = 35.3, wt.% (ζ') = 64.7, $\rho_{(\delta)}$ = 11.74 g/cm^3, $\rho_{(\zeta')}$ = 17.08 g/cm^3

$\rho_{(\text{eutectic})}$ = 100 g / Total volume of eutectic

$\rho_{(\text{eutectic})}$ = 14.72 g/cm^3

Density of Au-Sn eutectic "phase"

If Equation (1) is now solved for volume (area) percent of (ζ') primary phase using this value, the result is 7.94 area percent (ζ') primary phase. A similar calculation for the alloy on the Sn-rich side having a composition of 78.25 wt.% Au (21.75 wt.% Sn), would give a calculated primary (δ) phase weight percent of 9.94 wt.%, and conversion to area percent gives 12.13 percent (δ) primary phase.

A FORTRAN77 computer program was written and used to simplify these calculations so that a user only needs to know the following items:

1.) eutectic composition*

2.) wt.% of phase immediately above eutectic*

3.) wt.% of phase immediately below eutectic*

4.) density of phase immediately above eutectic†

5.) density of phase immediately below eutectic†

(* available from phase diagram)
(† available from JCPDS X-ray diffraction file)

Data Required to Use FORTRAN77 Program

The computer program allows the user to obtain either area % from wt.%, or wt.% from area %. The FORTRAN77 computer program used in this study is filed in the Department of Materials Science and Engineering at Lehigh University.

V. Results and Discussion

A. *Alloys Examined in the DSC and by Quantitative Metallography:*

Alloys used in the study are summarized in Table 1. Note that in one case a continuously cast alloy from Vendor 'X' was remelted and cooled rapidly to simulate cooling rates of previous samples made at Lehigh University. Alloys A, C, and E were originally intended to be cooled more rapidly than Alloys B, D, and F, but the actual cooling rates were approximately the same; therefore, alloys A & B, C & D, and E & F will be analyzed as though they were the same sample groups. Finally, the composition of alloys "A" & "B" are in question. For the purpose of analysis they will be considered slightly gold rich, but not as gold rich as alloys "E" & "F". The oil under which pure Au and Sn were submerged during melting was hydraulic grade (H-2), water white oil, viscosity = 300-325 (at 100 °F), flash point ~380-420 °C.

B. *Results of Quantitative Metallography:*

The results of the quantitative microstructural observations are summarized in Table 2, for the alloys described above. Examination of this table indicates good agreement between the expected and measured (δ) % in the eutectic for the 80 wt.% Au - 20 wt.% Sn continuous cast alloy and for Alloy "E". Alloy "A" gave an unusually high number for the (δ) % in the eutectic and this value is questioned as far as accurateness; however the value for % primary (ζ') for this same alloy appears to be reasonable in terms of visual comparison to this number.

The measured values of volume percent for primary (δ) phase appear to be in good agreement with those predicted for the Sn-rich alloys "C" and "D". The measured values of volume percent (ζ') phase for Au-rich alloys "A" and "E" are consistently high, much larger than the predicted value in each case.

The detailed analysis results for each alloy are provided on the pages following Table 2.

Summary of Au-Sn Alloys Used

Au-Sn Alloy Source	Weight %	Cooling Rate (Nominal)	Atmospheres
Vendor 'X' traditional cast	Au - 80 Sn - 20	slow	N_2 - H_2
Vendor 'X' continuous cast	Au - 80 Sn - 20	slow	N_2 - H_2
Vendor 'X' continuous cast (remelted)	Au - 80 Sn - 20	fast	glycerine (glycerol)
Alloy "A" & "B" Lehigh Univ.	Au - 80 Sn - 20	fast	oil
Alloy "C" & "D" Lehigh Univ.	Au - 78.25 Sn - 21.75	fast	oil
Alloy "E" & "F" Lehigh Univ.	Au - 80.87 Sn - 19.13	fast	oil

TABLE 1: Summary of Au-Sn Alloys Used in This Study

Summary of Microstructural Observations
Area Percent Measurements

wt.% Au "ID"	% Eutectic (δ) Measured	1σ	% Eutectic (δ) Predicted	% Primary (δ) Measured	1σ	% Primary (δ) Predicted	% Primary (ζ') Measured	1σ	% Primary (ζ') Predicted
78.25 "C"	†	†	44.2	13.9	3.1	12.13	0	0	0
78.25 "D"	†	†	44.2	14.8	1.8	12.13	0	0	0
80 concast.	45.2	2.6	44.2	0	0	0	0	0	0
80 concast. remelted	†	†	44.2	†	†	0	†	†	0
80 trad. cast	†	†	44.2	†	†	0	†	†	0
80 (?) "A"	65.8*	3.6	44.2	0	0	0	8.0	1.2	0
80.87 "E"	44.0	1.0	44.2	0	0	0	15.5	1.8	7.94

† Indicates Measurement Not Made

* Measurement is Suspect

1σ = Standard Deviation Associated with Measurement in Previous Column

TABLE 2: Summary of Microstructural Observations

For the readers convenience the following table summarizes the locations of the various microstructures and the quantitative image analysis results for each alloy:

Alloy ID	OPTICAL Micrographs (fig. # / page #)	DIGITAL COMPUTER Images (fig. # / page #)	Summary Analysis (fig. # / page #)
Alloy "C" 78.25% Au	12 / 43	13 / 44	14 / 45
Alloy "D" 78.25% Au	15 / 46	16 / 47	17 / 48
Vendor 'X' Continuous Cast 80% Au	†	18, 19 / 49, 50	20 / 51
Vendor 'X' Continuous Cast (Remelted) 80% Au	21 / 52	†	†
Alloy "A" 80% Au	22 / 53	23, 24 / 54-56	25 / 57
Alloy "E" 80.87% Au	26 / 58	27, 28 / 59-61	30 / 62

† Photos not taken or analysis not complied

TABLE 3: Summary of Image and Data Locations

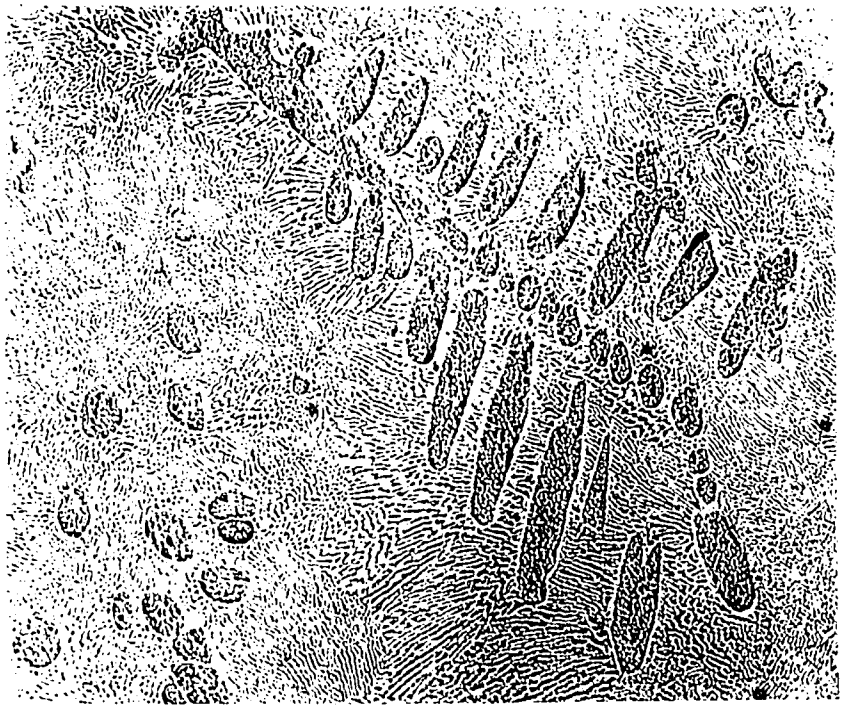

FIGURE 12: Alloy "C" (78.25 wt.% Au - 21.75 wt.% Sn)
Primary (δ') phase (light) amidst eutectic phase.
Light optical microscopy (500X).

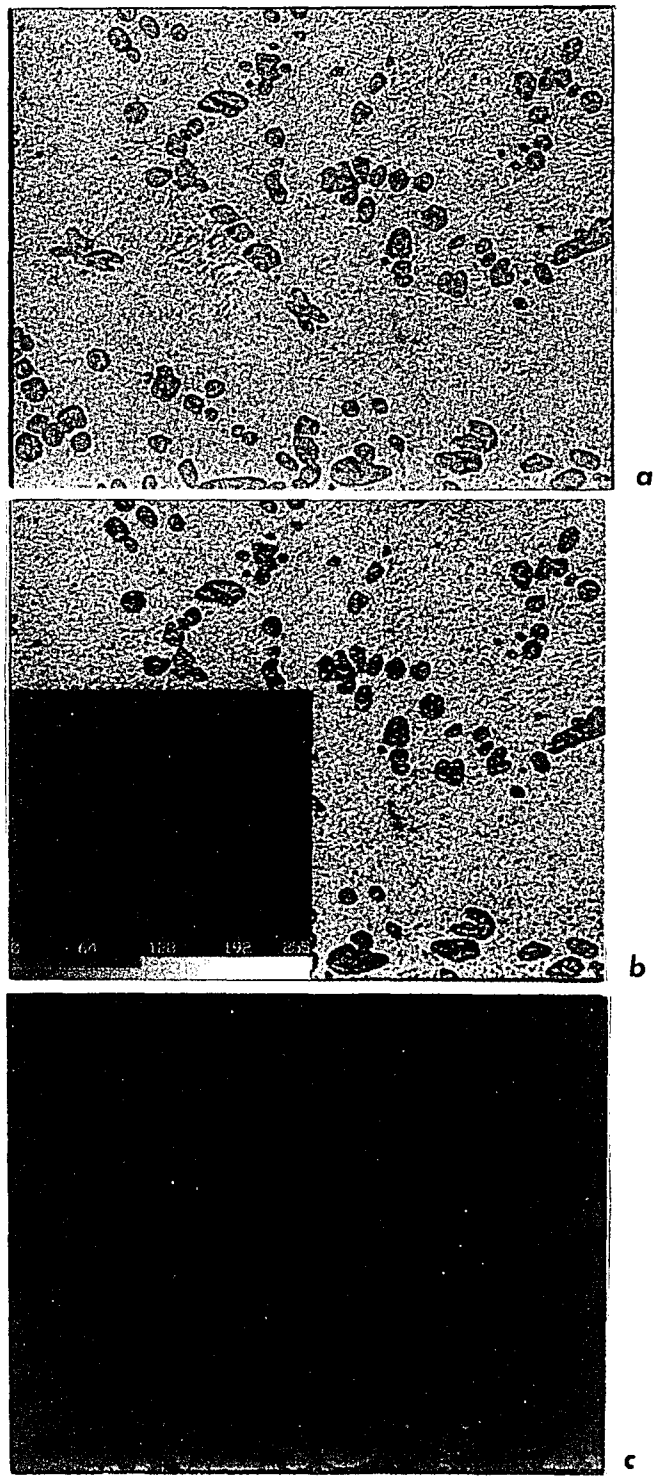

FIGURE 13: a.) Digital computer image of Alloy "C" (78.25 wt.% Au - 21.75 wt.% Sn) (156X).

b.) Computer Enhanced Image (156X).

c.) Microstructure area percentage selected for analysis by the computer (156X).

SPECIMEN ID: *SAMPLE "C" (78.25% Au - 21.75% Sn)*
Rapid Cooling (air)

Trial	% Primary DELTA Phase Observed:
1	15.006
2	15.4152
3	13.5889
4	15.4837
5	9.4143
6	11.4306
7	16.1685
8	13.1923
9	17.574
10	11.9573

Average Percent of PRIMARY DELTA Phase Observed:	13.9
Standard Deviation (1 sigma):	3.1
Percent of PRIMARY DELTA Phase Predicted:	12.13
% Difference:	14.8

FIGURE 14: Summary of Image Analysis Data for Sample "C" (78.25 wt.% Au - 21.75 wt.% Sn)

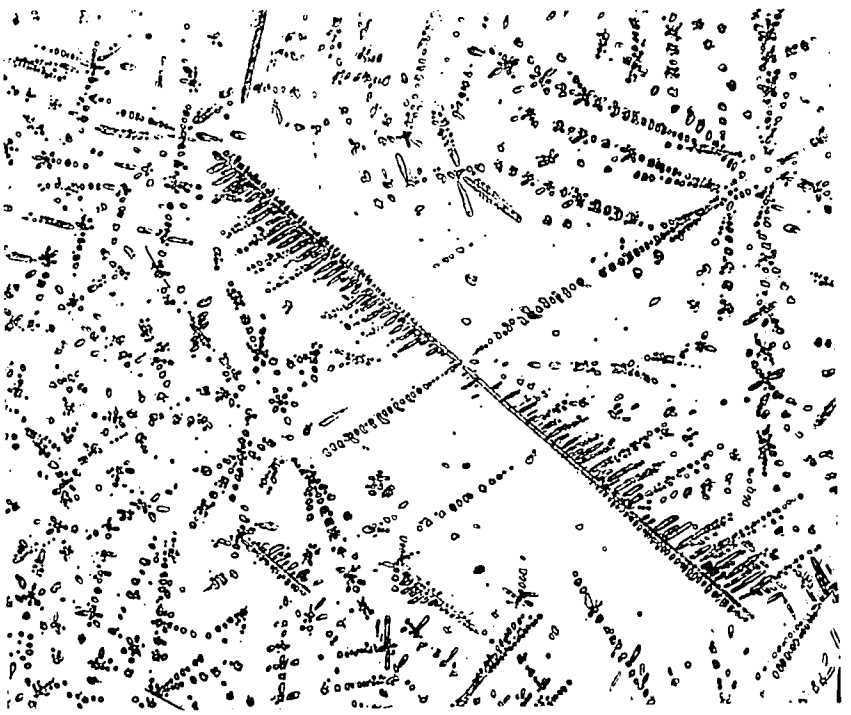

FIGURE 15: Alloy "D" (78.25 wt.% Au - 20.25 wt.% Sn).
Primary (δ') phase (dark) amidst eutectic phase.
Light optical microscopy (100X).

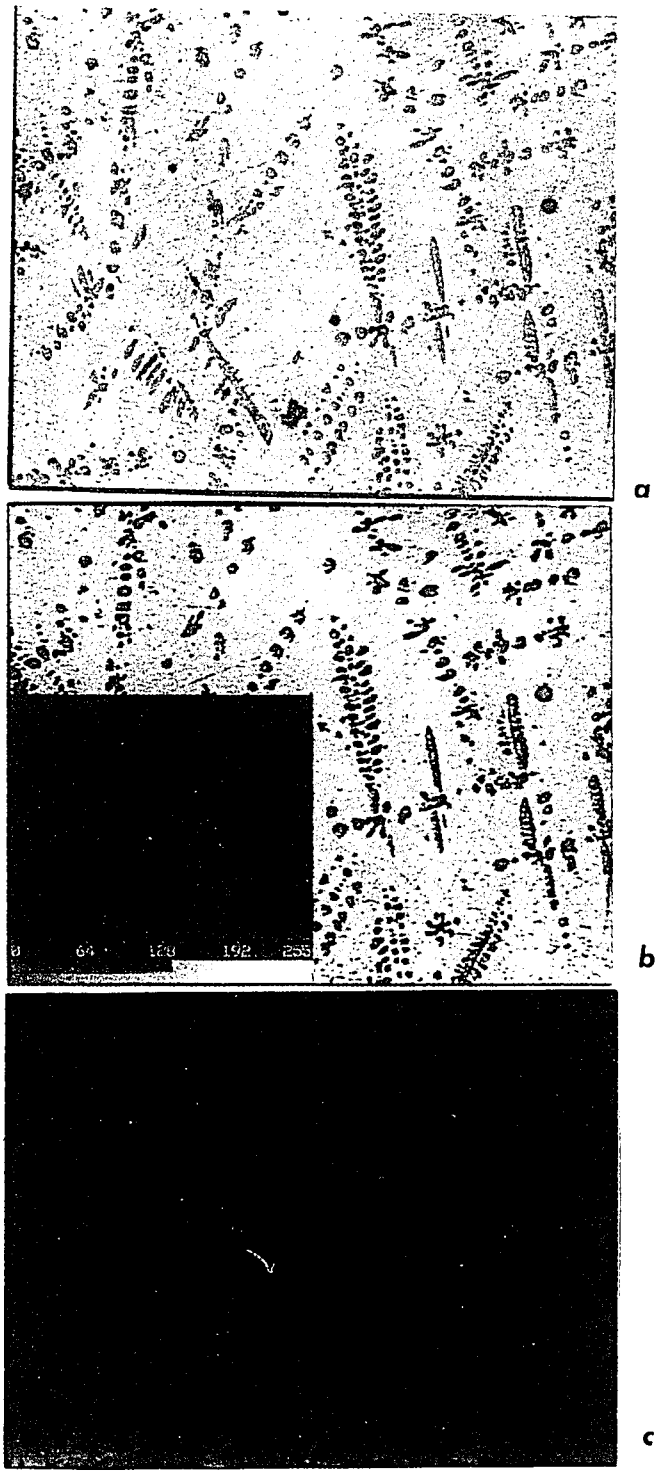

FIGURE 16: a.) Digital computer image of Alloy "D" (78.25 wt.% Au - 21.75 wt.% Sn) (156X).

b.) Computer Enhanced Image (156X).

c.) Microstructure area percentage selected for analysis by the computer (156X).

SPECIMEN ID: *SAMPLE "D" (78.25% Au - 21.75% Sn)*
Rapid Cooling (air)

Trial	% Primary DELTA Phase Observed:
1	15.8753
2	14.6454
3	15.5567
4	15.1023
5	14.8352
6	14.8395
7	14.9084
8	13.5486
9	14.2311
10	14.0957

Average Percent of PRIMARY DELTA Phase Observed:	14.8
Standard Deviation (1 sigma):	1.8
Percent of PRIMARY DELTA Phase Predicted:	12.13
% Difference:	21.7

FIGURE 17: Summary of Image Analysis Data for Sample "D" (78.25 wt.% Au - 21.75 wt.% Sn)

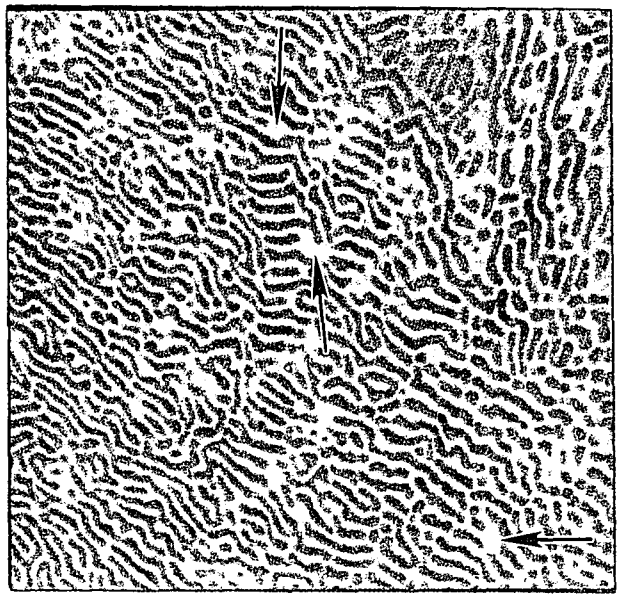

a

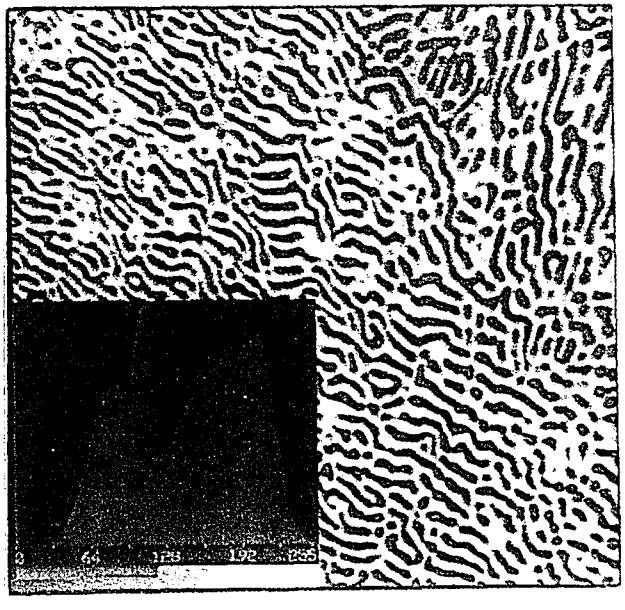

b

FIGURE 18: a.) Digital computer image of Vendor 'X' Continuous Cast (80 wt.% Au - 20 wt.% Sn) Alloy (2000X). Arrow points to possible primary (ζ') phase.

b.) Microstructural area percentage selected for analysis by the computer (2000X).

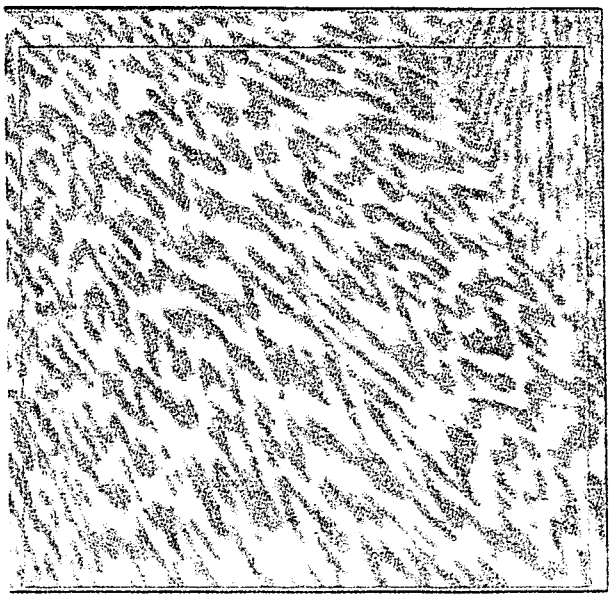

a

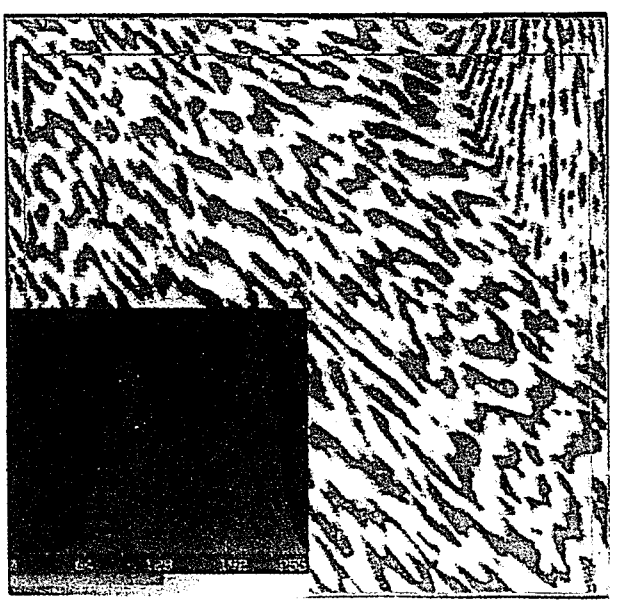

b

FIGURE 19: a.) Digital computer image of Vendor 'X' Continuous Cast (80 wt.% Au - 20 wt.% Sn) Alloy (2000X).

b.) Microstructure area percentage selected for analysis by the computer (2000X).

SPECIMEN ID: *Vendor 'X' (Continuous Cast)*
X-section parallel to RD

Trial #:	% DELTA Phase Observed:
1	43.4906
2	44.7174
3	49.9286
4	48.5342
5	42.8937
6	49.6454
7	43.1761
8	39.3812
9	43.9393
10	48.4491
11	44.0743
12	44.1475

Average Percent of DELTA Phase Observed:	45.2
Standard Deviation (1 sigma):	2.6
Percent of DELTA Phase Predicted:	44.2
% Difference:	2.3

FIGURE 20: Summary of Image Analysis Data for Vendor 'X' -- Continuous Cast (80 wt.% Au - 20 wt.% Sn)

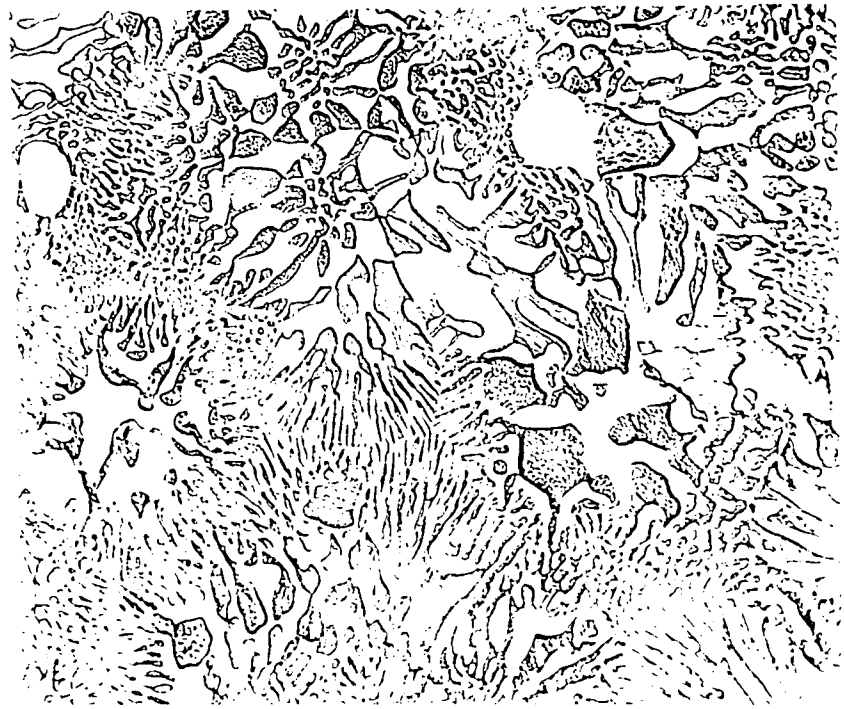

FIGURE 21: a.) Vendor 'X' Continuous Cast (80 wt.% Au - 20 wt.% Sn) Remelted Alloy.. Primary (ζ') phase (light) and primary (δ) phase (dark) with eutectic interlaced. Light optical microscopy (625X).

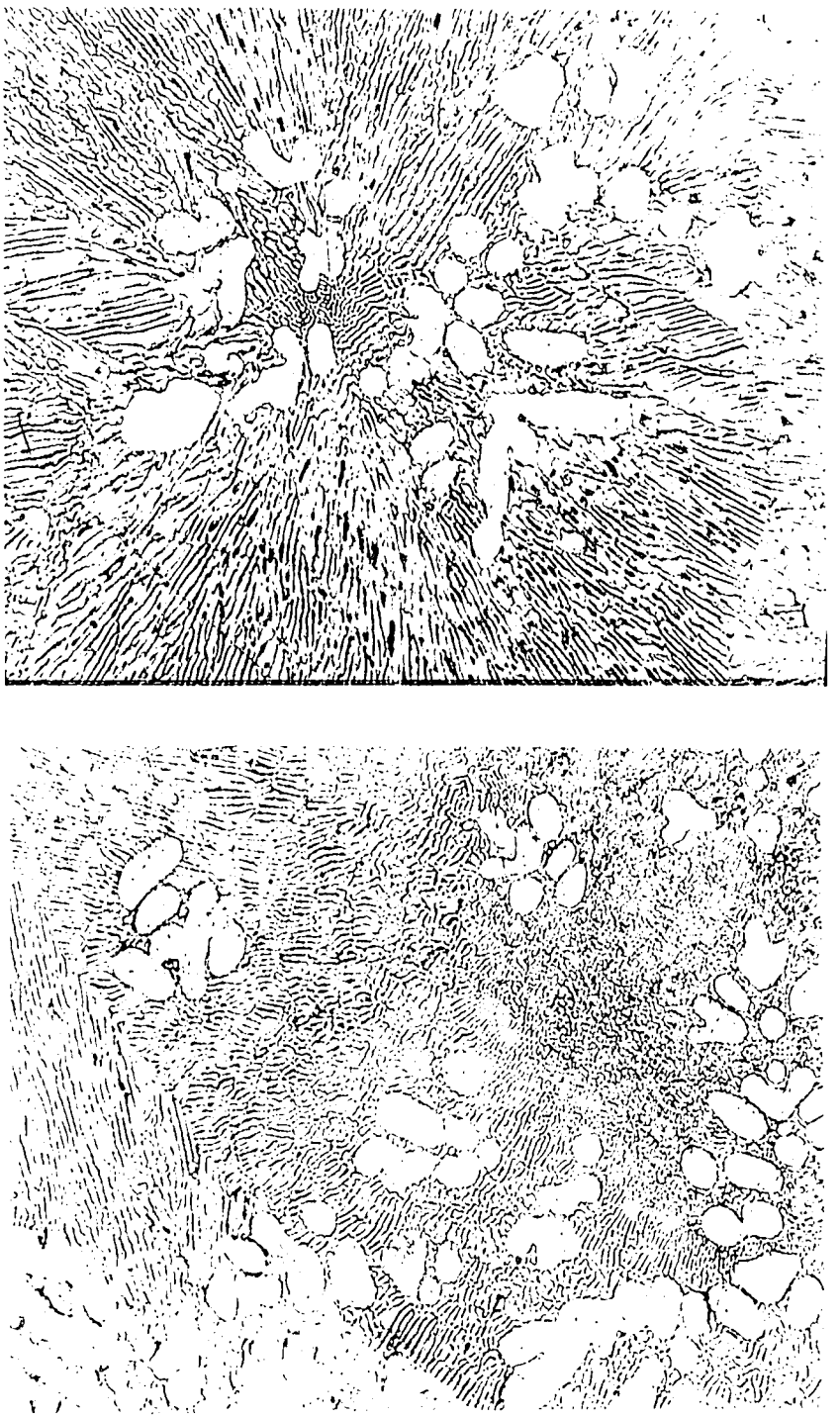

FIGURE 22: a & b.) Alloy "A" (80 wt.% Au -20 wt.% Sn). Primary (ζ') phase (light) amidst eutectic phase. Light optical microscopy (500X).

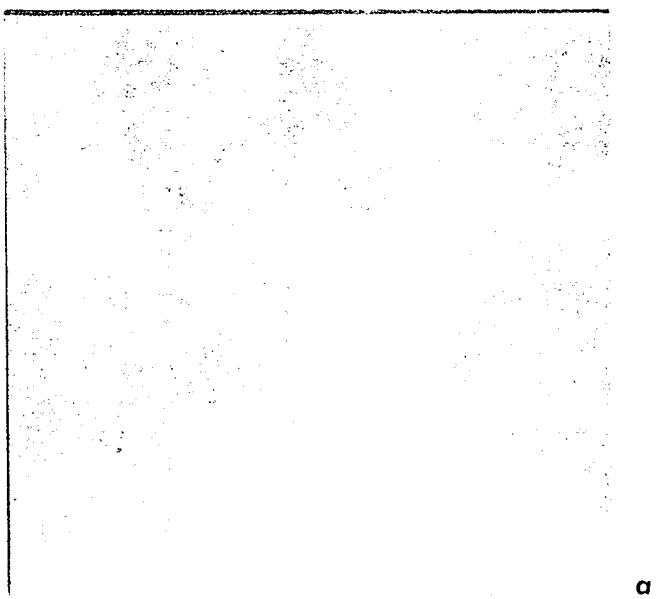

FIGURE 23: a.) Digital computer image of Alloy "A" (80 wt.% Au - 20 wt.% Sn) (125X).

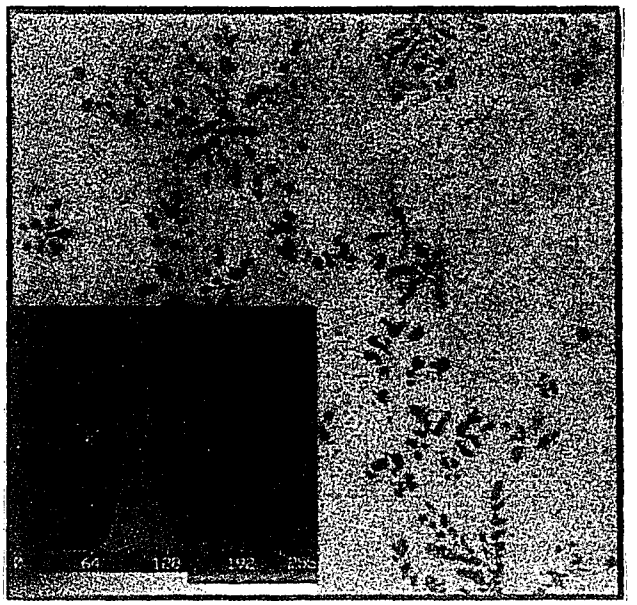

b

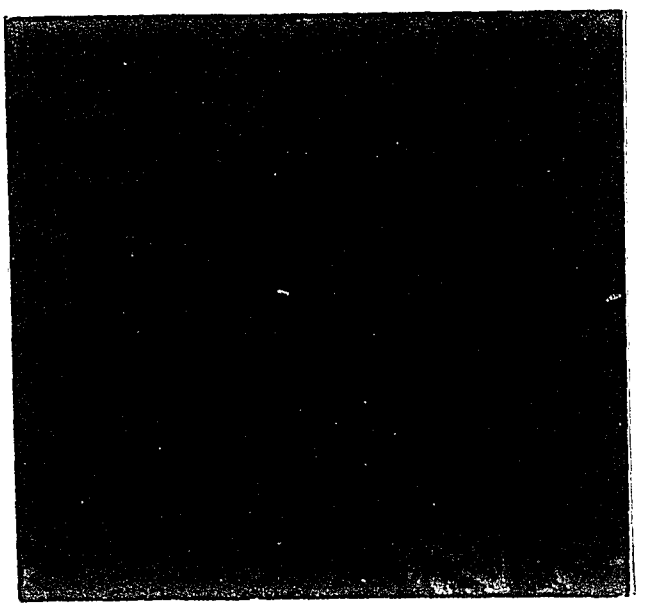

c

FIGURE 23: b.) Enhanced digital image (125X).

c.) Microstructure area percentage selected for analysis by the computer (125X). Smallest particles excluded from analysis

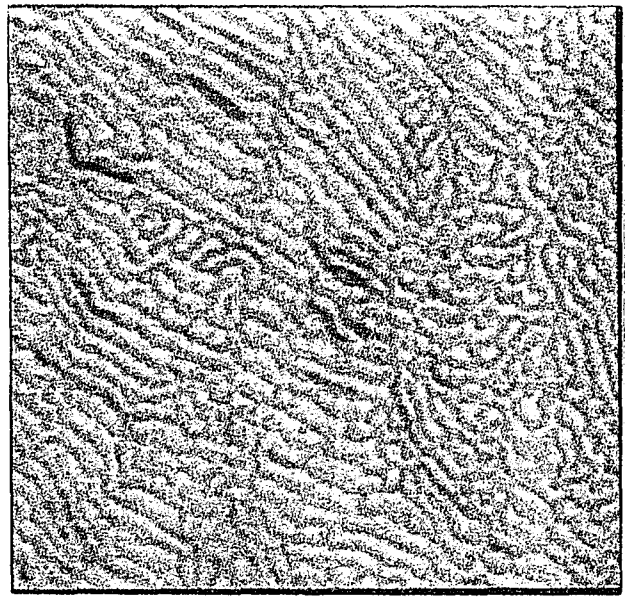

a

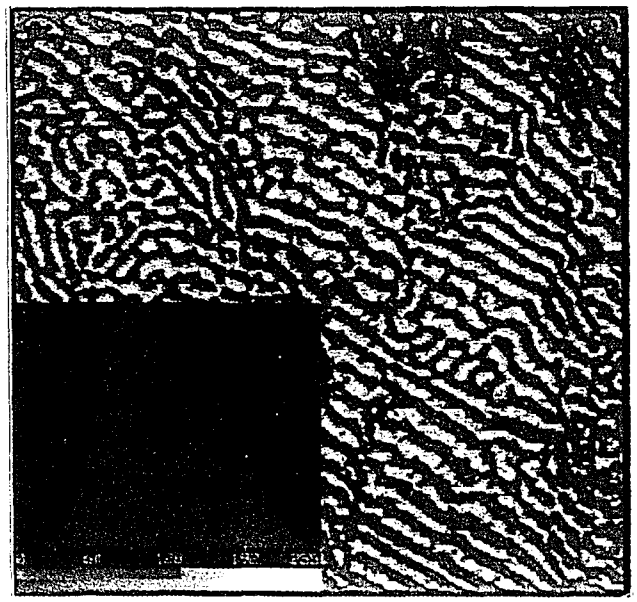

b

FIGURE 24: a.) Digital computer image of Alloy "A" (80 wt.% Au - 20 wt.% Sn) (2000X).

b.) Microstructure area percentage selected for analysis by the computer (2000X).

SPECIMEN ID:	*SAMPLE "A" (80% Au - 20% Sn)* *Rapid Cooling (air)*

Trial	% DELTA Phase Observed* :	% Primary ZETA PRIME Phase Observed:
1	58.4021	8.3942
2	64.1837	4.4995
3	67.5191	7.5669
4	76.4442	9.4312
5	70.412	7.2574
6	66.6411	6.7191
7	62.8755	8.419
8	64.9585	9.6722
9	63.4072	9.3214
10	62.9139	8.4533

Average Percent of PRIMARY ZETA PRIME Phase Observed:	8.0
Standard Deviation (1 sigma):	1.2
Percent of PRIMARY ZETA PRIME Phase Predicted:	0
% Difference:	100.0
Average Percent of DELTA Phase observed* :	65.8
Standard Deviation (1 sigma):	3.6
Percent of DELTA Phase Predicted:	44.2
% Difference:	48.8

* *Measurement is suspect*

FIGURE 25: Summary of Image Analysis Data for Sample "A" (80 wt.% Au - 20 wt.% Sn)

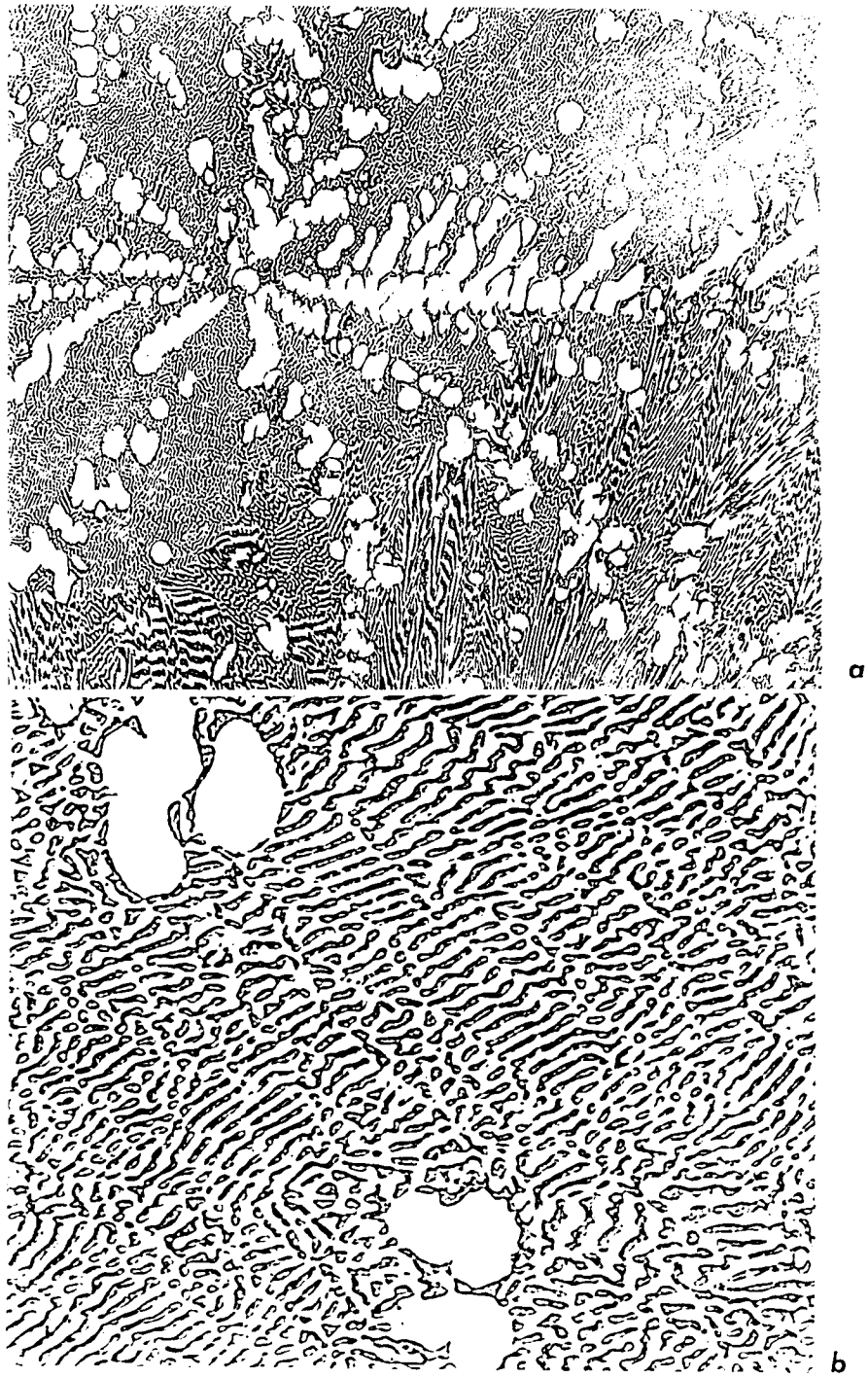

FIGURE 26: a.) Alloy "E" (80.87 wt.% Au - 19.13 wt.% Sn).
Primary (ζ') phase (light) amidst eutectic phase.
Light optical microscopy (250X).

b.) Alloy "E" (80.87 wt.% Au - 19.13 wt.% Sn)
Primary (ζ') phase (light) amidst eutectic phase.
Light optical microscopy (1000X).

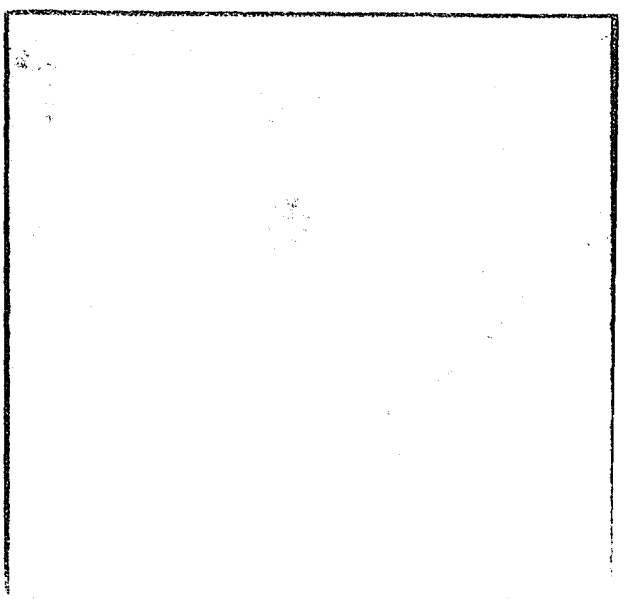

FIGURE 27: a.) Digital computer image of Alloy "E" (80.87 wt.% Au - 19.13 wt.% Sn) (156X).

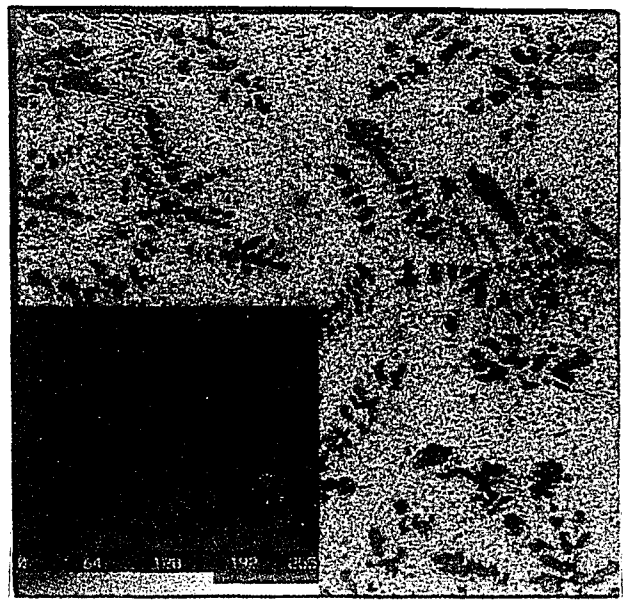

b

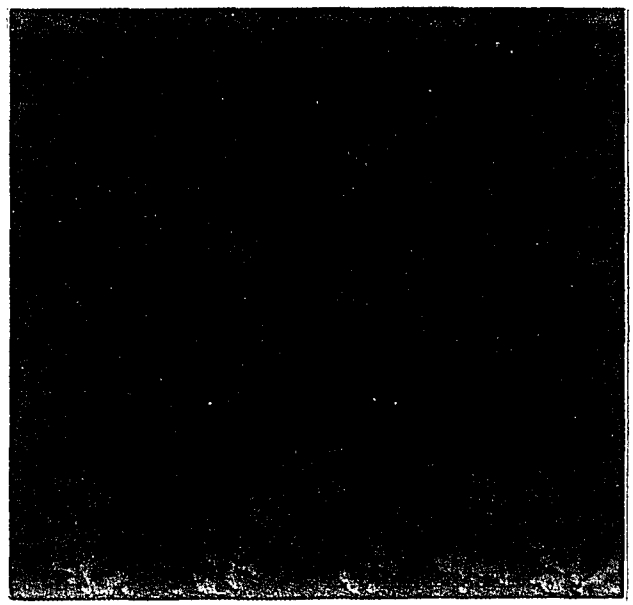

c

FIGURE 28: b.) Enhanced digital image (156X).

c.) Microstructure area percentage selected for analysis by the computer (156X). Smallest particles excluded from analysis (See Procedures section for a full explanation of digital image selection and analysis).

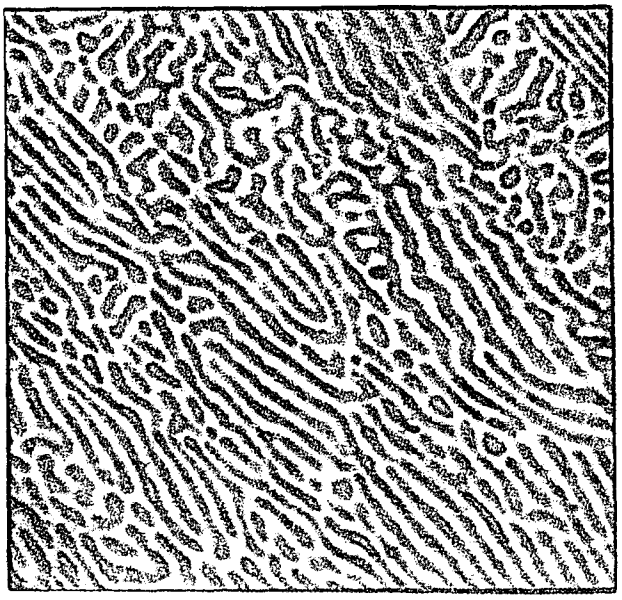

a

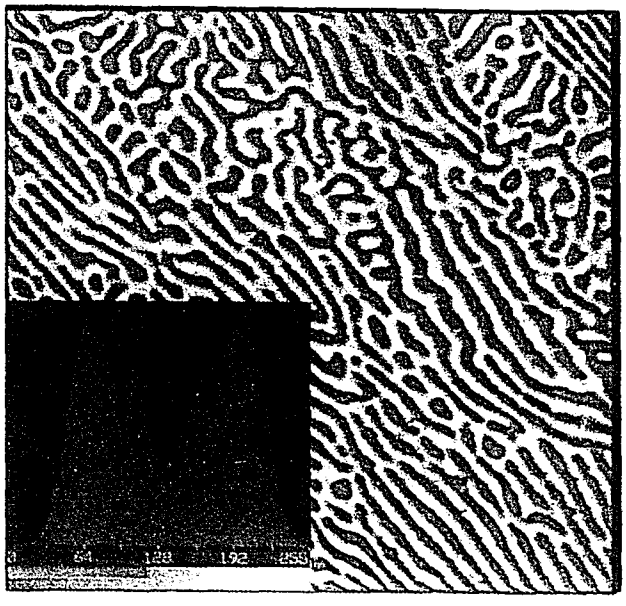

b

FIGURE 29: a.) Digital computer image of Alloy "E" (80.87 wt.% Au - 19.13 wt.% Sn) (2000X).

b.) Microstructure area percentage selected for analysis by the computer (2000X). (See Procedures section for a full explanation of digital image selection and analysis).

SPECIMEN ID:	*SAMPLE "E" (80.87% Au - 19.13% Sn) Rapid Cooling (air)*	
Trial	% DELTA Phase Observed:	% Primary ZETA PRIME Phase Observed:
1	42.0277	17.7548
2	41.5784	14.2592
3	45.0035	12.8966
4	44.9882	13.5789
5	43.2545	19.1232
6	45.091	13.9195
7	43.5645	19.5257
8	44.8239	14.6299
9	44.244	15.4654
10	45.0266	14.5011
11		14.9412

Average Percent of PRIMARY ZETA PRIME Phase Observed:	15.5
Standard Deviation (1 sigma):	1.8
Percent of PRIMARY ZETA PRIME Phase Predicted:	7.94
% Difference:	95.3

Average Percent of DELTA Phase observed:	44.0
Standard Deviation (1 sigma):	1.1
Percent of DELTA Phase Predicted:	44.2
% Difference:	0.5

FIGURE 30: Summary of Image Analysis Data for Sample "E" (80.87 wt.% Au - 19.13 wt.% Sn)

C. Continuous Casting Structure:

The microstructure typical of the continuously cast Au-Sn eutectic alloy is shown in Figure 31 (40X). This micrograph is taken longitudinal to the growth direction and shows the eutectic "grains" or colonies and their individual growth directions. Although it appears that the eutectic is nucleated at the top and bottom of the mold wall, inward growth then tends to curve around opposite to the growth direction, as might be expected. Inspection of the figure shows two curved traces which are believed to be related to the stepped pitch of the cast bar. Solidification would be expected to be everywhere perpendicular to the growth front and this appears to be the case here. The high magnification photomicrographs shown in Figures 18 and 19 indicate the fine size of the eutectic interlamellar spacing for the material.

It is interesting to note that this material is sometimes fabricated by rapid solidification methods because of its susceptibility to brittle failure. Humpston and Jacobson [25] indicate that: "Although difficult, this solder can be hot rolled to foil and preforms stamped from it. By using rapid solidification casting technology, it is possible to produce thin ductile foil, up to about 75μm thick and, having an amorphous microstructure. However, the amorphous state is somewhat unstable, and within about 30 minutes at room temperature, the rapidly solidified strip is indistinguishable in its mechanical properties from foil prepared by conventional fabrication methods [Mattern, 1989]. Nevertheless, this crystallization can be suppressed for about a year if the quench-cooled material is stored under liquid nitrogen (-196 °C) and for close to one month at (-20 °C), so that it is possible to manufacture shaped foil preforms while the

(DIRECTION OF INGOT REMOVAL FROM CASTER)

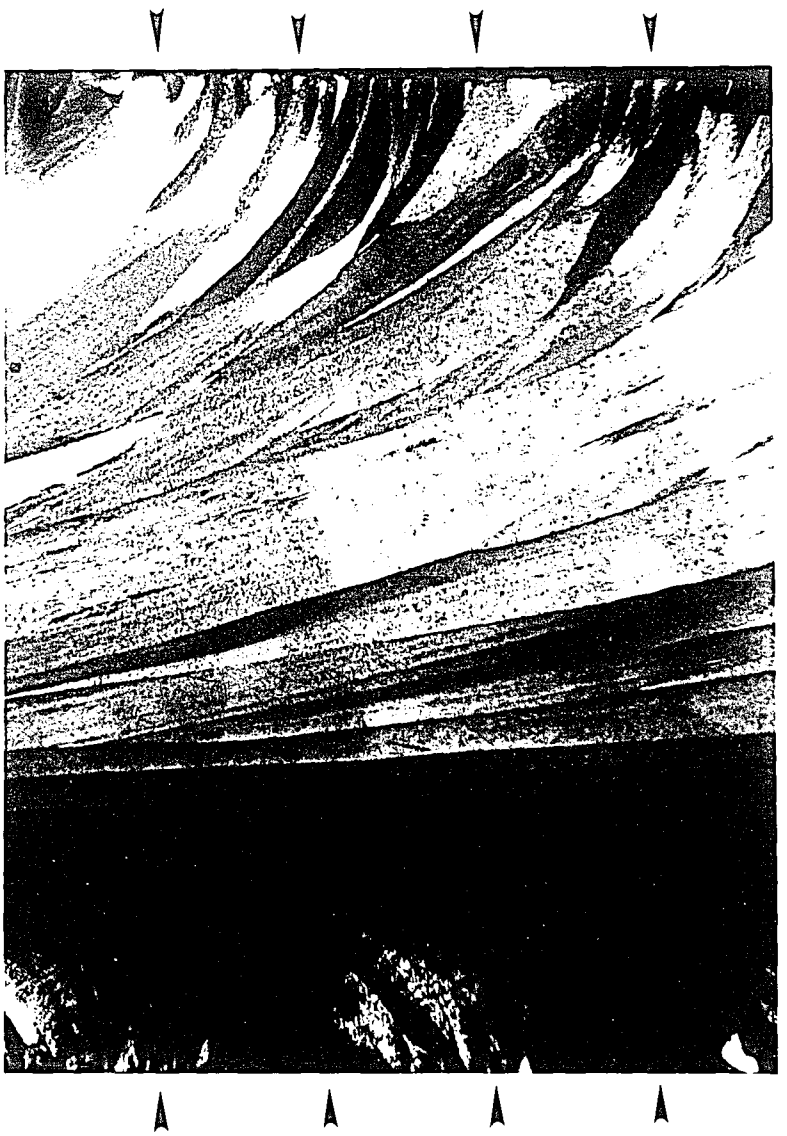

FIGURE 31: Microstructure of Continuous Cast Bar
Optical Microscopy -- Polarized Light (40X)
(Arrowheads point to outside edges of ingot)

strip is still ductile, which can then be either immediately placed in a jig or returned to cold storage."

D. Initial DSC Experiments:

A comprehensive study was made in an attempt to replicate the spurious peak (shoulder) which had previously been reported as being appeared attached to the main DSC eutectic melting peak of an Au-Sn solder [7]. In the present study many eutectic alloy samples were evaluated in the DSC in an attempt to reproduce the shoulder. In order to evaluate if contamination was causing the appearance of the shoulder some alloys were cleaned with solvents and others were not. In some cases the amount of material tested was doubled to see if any results were exaggerated. The heating and cooling rates in all cases were to heat from ingot at 10 °C / min., then cool at 100 °C / min., then heat at 10 °C / min., then cool at 100 °C / min. Table 4 shows the results of these initial DSC experiments. Although we were able to obtain such a shoulder, the appearance of the shoulder was very unpredictable, i.e., sometimes it appeared and sometimes it did not.

No trends were immediately evident from these initial DSC test results. The conclusion was that the source of the alloy does not appear to be a factor in the appearance of the shoulder, nor does cleaning procedure appear to be a factor either.

It was therefore hypothesized that the shoulder on the DSC peak was related to the solidification process itself. The presence of residual Au-Sn intermetallic phases after casting is also not consistent with present x-ray diffraction results nor is it expected based on the actual melting process.

Inspection of the Au-Sn phase diagram indicates both the epsilon phase (ε) and eta phase (η) to both be Sn rich phases, that is they lie above 50 wt.% Sn. Both (ε) and (η) were previously reported [7] as suspect intermetallic phases because is was believed that the following casting procedure was followed:

1.) Melt pure Sn (T_m = 231.96 °C).
2.) Add scrap material.
3.) Add pure Au (T_m = 1064.43 °C) until desired eutectic composition is reached.

Assumed Casting Procedure

Because pure Sn has a T_m below (ε) and (η) it is possible to assume that these phases might not melt if they were present in the scrap or created during the casting process [7].

However, key pieces of evidence refute this theory. First, the actual casting procedure which is used to make Au-Sn eutectic alloy starts by melting pure Au, and therefore processing starts from the Au-rich side of the Au-Sn phase diagram. Second, because T_m for Au is much greater than T_m for either (ε) or (η) it would be unlikely for these phases to exist in the final product even if they were present in the scrap to begin with.

Alloy	Manufacturer	Weight (* = 20-25 mg)	Cleaning (* = acetone then trichlorethylene)	Observations
Pure Sn	Aesar	*	none	normal peak
Pure Sn	Aesar	50 mg	none	normal peak
Au-Sn (eut.)	Vendor 'X'	*	*	no shoulder
Au-Sn (eut.)	Vendor 'Y'	*	*	no shoulder
Au-Sn (eut.)	Vendor 'X'	*	*	no shoulder
Au-Sn (eut.)	Vendor 'X'	*	*	Add'l. peak on 2nd cooling
Au-Sn (eut.)	Vendor 'Y'	*	*	no shoulder
Au-Sn (eut.)	Vendor 'Y'	50 mg	*	Shoulder on heating, add'l. peaks on cooling
Au-Sn (eut.)	Vendor 'X'	50 mg	*	Shoulder on heating and add'l. peaks on cooling
Au-Sn (eut.)	Vendor 'X'	*	none	Add'l. peak on 2nd cooling
Au-Sn (eut.)	Vendor 'Y'	*	none	no shoulder
Au-Sn (eut.)	Vendor 'Y'	*	*	Add'l. peak on 2nd cooling
Au-Sn (eut.)	Vendor 'X'	*	*	Shoulder on 2nd heating and add'l. peaks on cooling.
Au-Ge	Vendor 'X'	*	none	no shoulder
Au-Si	Vendor 'X'	*	none	no shoulder
Au-Ge	Vendor 'X'	*	*	no shoulder
Au-Ge	Vendor 'X'	50 mg	none	no shoulder
Au-Sn (eut.)	Vendor 'Y'	*	none	no shoulder
Au-Sn (eut)	Vendor 'Y'	*	Acetone only	no shoulder
Au-Sn (eut.)	Vendor 'Y'	*	Trichlor. only	no shoulder
Au-Sn (eut.)	Vendor 'Y'	*	*	Shoulder on 2nd heating and add'l. peaks on cooling

Table 4: Initial DSC Results

E. *Undercooling Effect in Sn:*

If a sample of pure Pb (or Au) were tested using DSC, it typically shows little or no undercooling at the thermal scan rates commonly used. Therefore, the measured value for the melting point would be the same if the measurement were made during heating or cooling. However, pure Sn appears to behave quite differently in that upon cooling the measured melting point of Sn is usually depressed, and this is explained by the large undercooling tin experiences when cooled rapidly. Note the melting point depression, nearly 40 °C, on the DSC cooling curve of pure Sn (Figure 32) as compared to the position of the peak on heating (Figure 33). This large undercooling effect has bee found to be a common feature of all the tin based alloys studied in the present investigation.

F. DSC Results for Alloys Studied:

A summary of the results of DSC measurements for the alloys studied (Table 1) are given in Table 5. The individual DSC scans for second heating and second cooling are provided for each alloy on pages 72 to 84 following Table 5. For Alloy "E" the first heating curve is also included because it has a slightly more apparent shoulder on the high temperature side of the main melting peak than does the second heating curve.

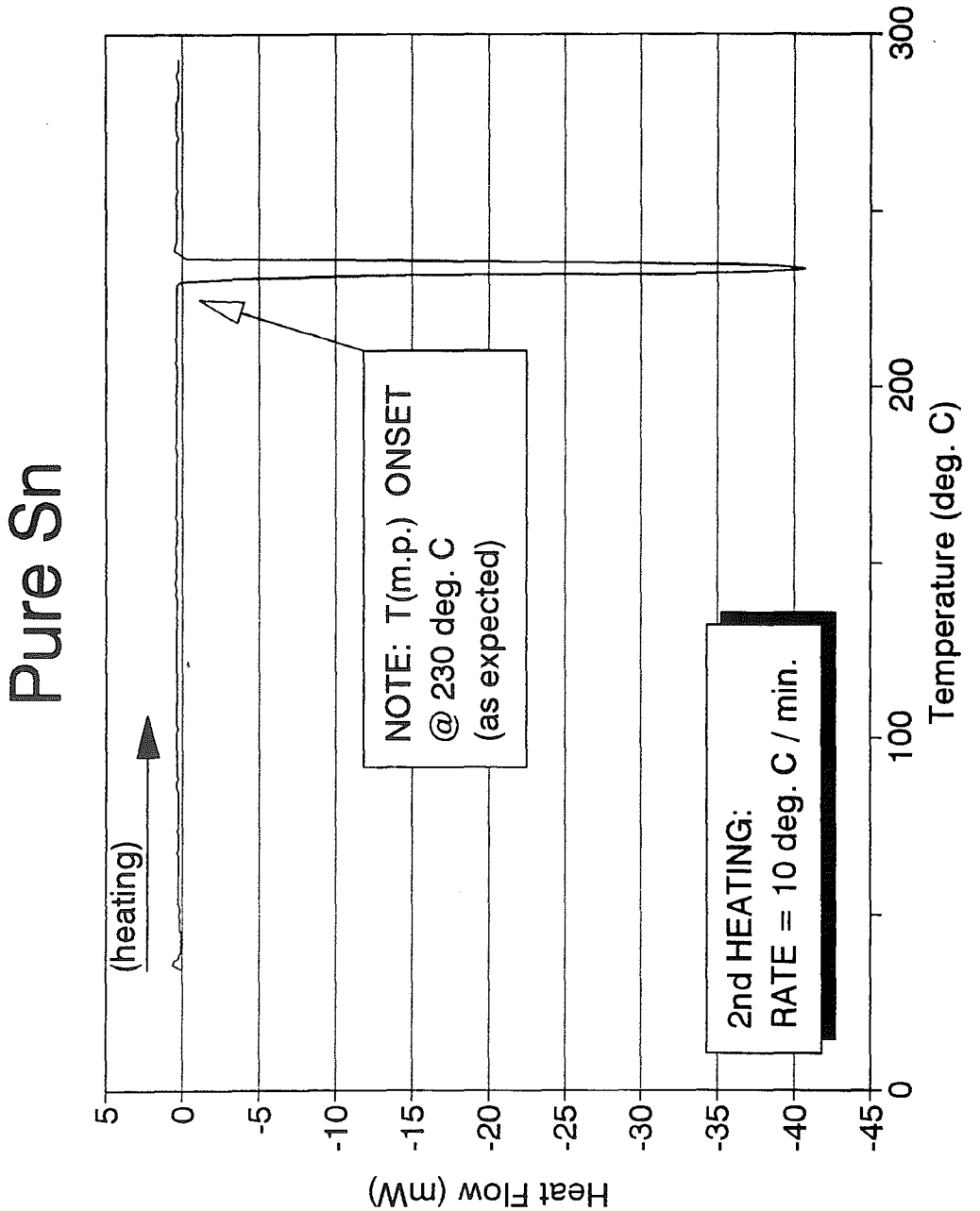

FIGURE 32: DSC Trace for Pure Sn.
2nd Heating at 10° C / min. from 35° C to 300° C.

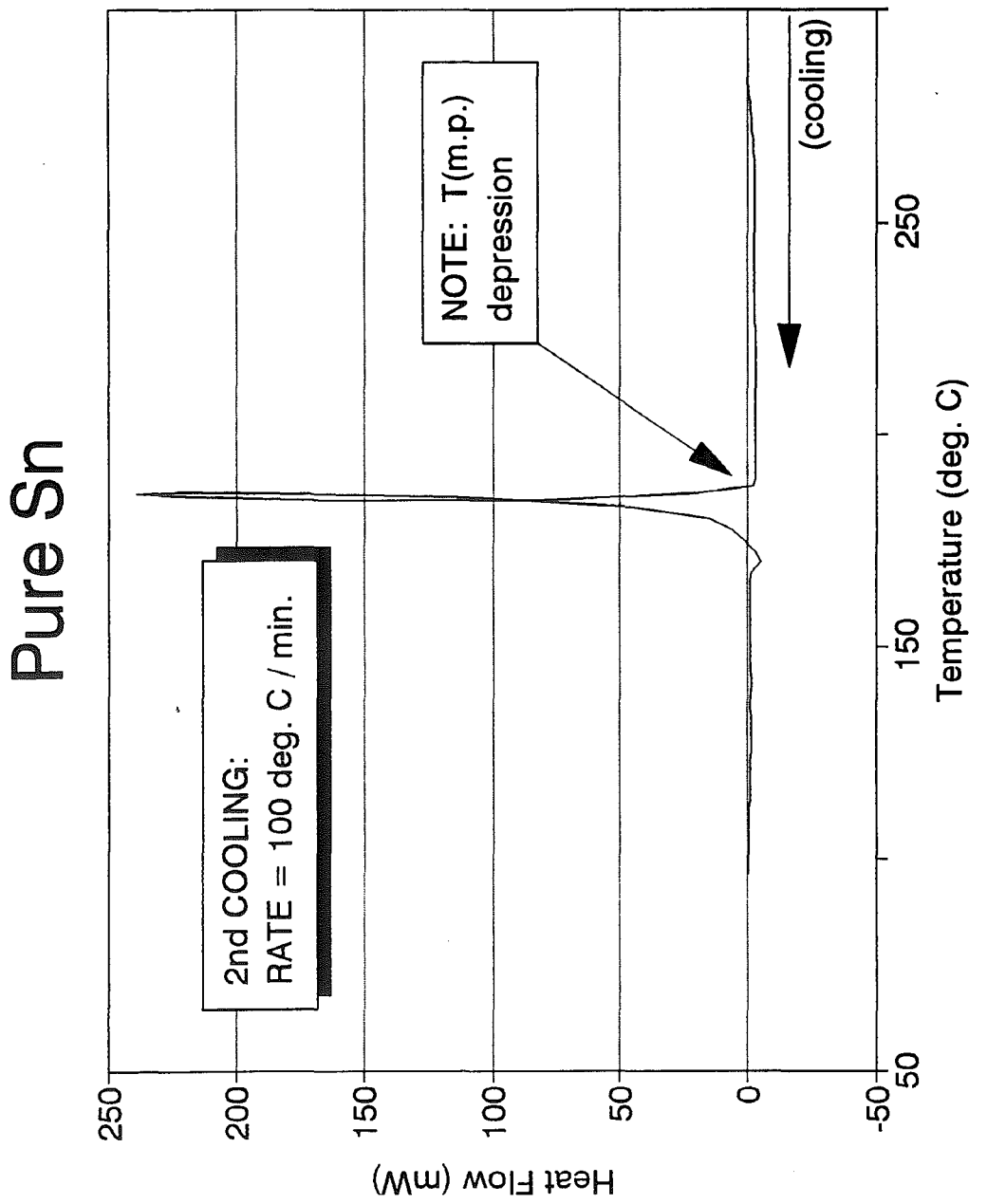

FIGURE 33: DSC Trace for Pure Sn.
2nd Cooling at 100° C / min. from 300° C to 35° C.

Summary of DSC Observations

Eutectic = Eutectic Temperature (°C)
Liquid = Liquidus Temperature (°C)

wt.% Au	Heating Eutectic (°C)	Heating Liquid (°C)	Cooling Eutectic (°C)	Cooling Liquid (°C)	U.Cooling Eutectic (°C)	U.Cooling Liquid (°C)	Liquid †
76*	281	328	270	303	11	25	320
78*	282	299	272	277	10	22	300
78.25 Alloy "D"	280+	300-	272	295	8	5	300-
80*	282	none	254	282	28	--	--
80 concast	280	none	210	none	70	--	--
80 concast remelt	280	none	275	none	5	--	--
80 trad. cast	280	none	260	none	20	--	--
80+ Alloy "A"	280	320-	277	315	none	10	?
80.87 Alloy "E"	280	320-	280	315	none	5	320-
81*	281	319	220	264	61	55	320
84*	280	460	274	442	6	18	460

* Indicates Data From IBM Study (Unpublished) [26].

† Liquidus Temperature (°C) Predicted by Phase Diagram [6]

+/- Following a number means the true value is a small amount greater/less than the amount shown,

---

TABLE 5: Summary of DSC Observations

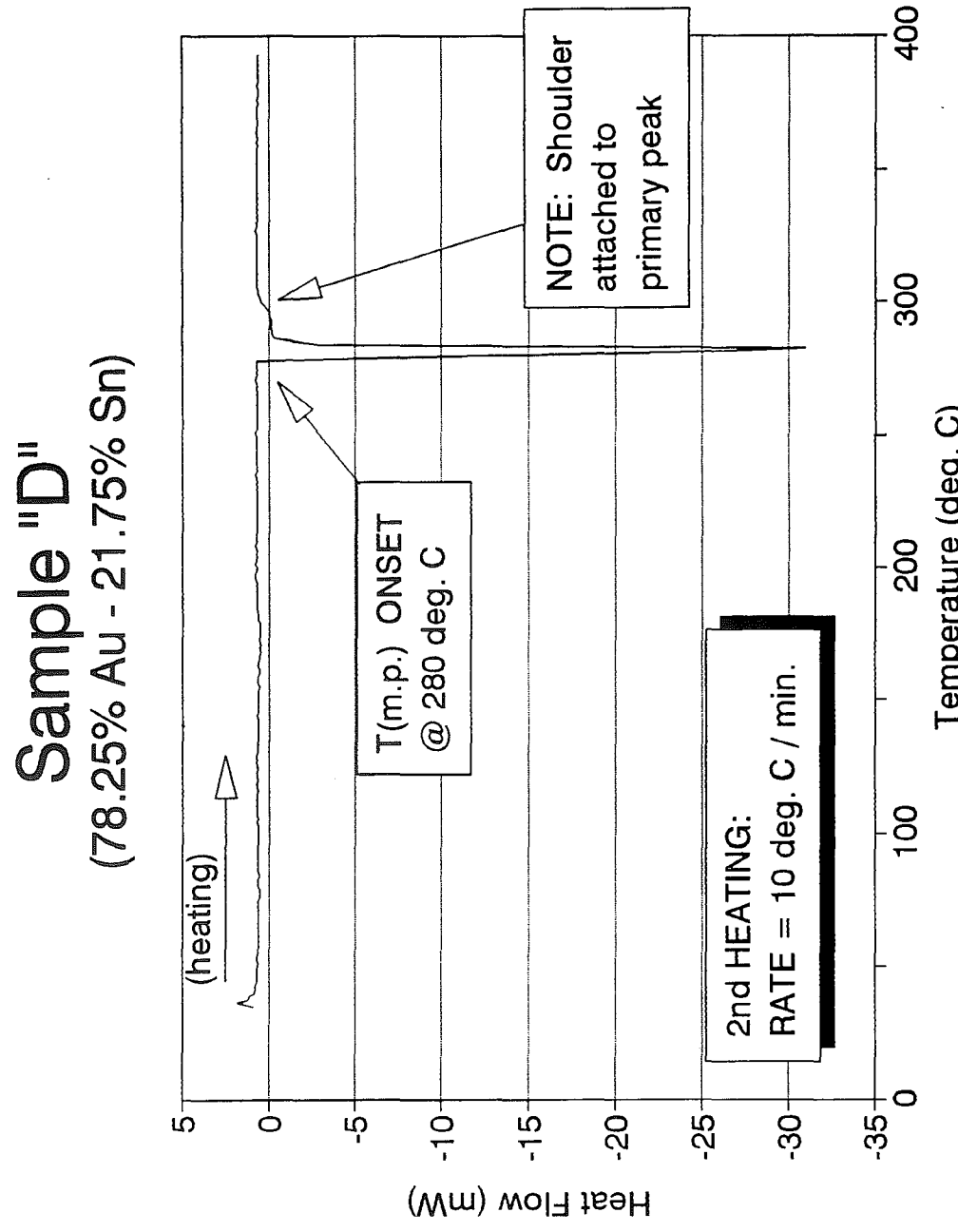

FIGURE 34: DSC Trace for Sample "D" (78.25% Au - 21.75% Sn). 2nd Heating at 10° C / min. from 35° C to 400

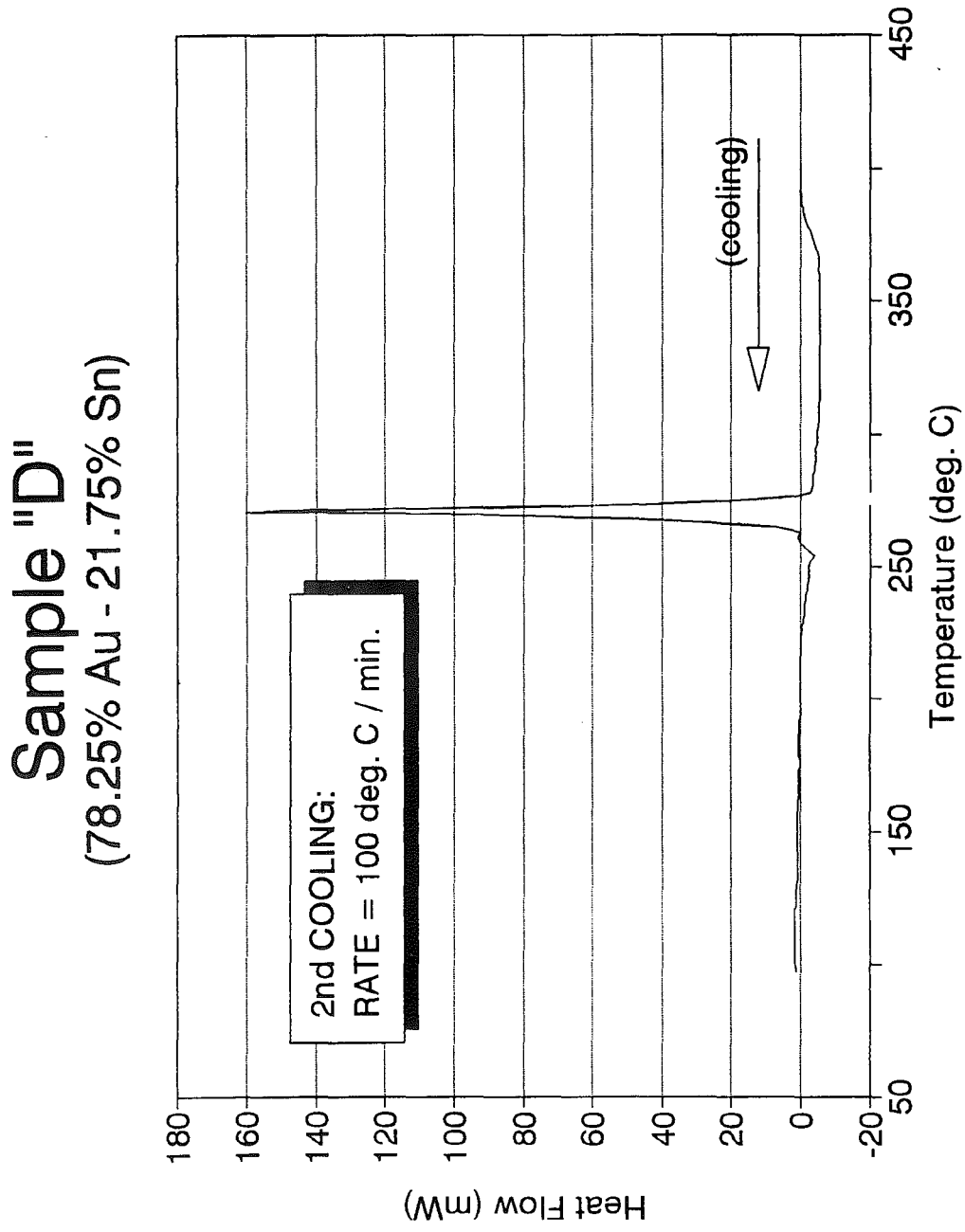

FIGURE 35: DSC Trace for Sample "D" (78.25% Au - 21.75% Sn). 2nd Cooling at 10° C / min. from 400° C to 35° C.

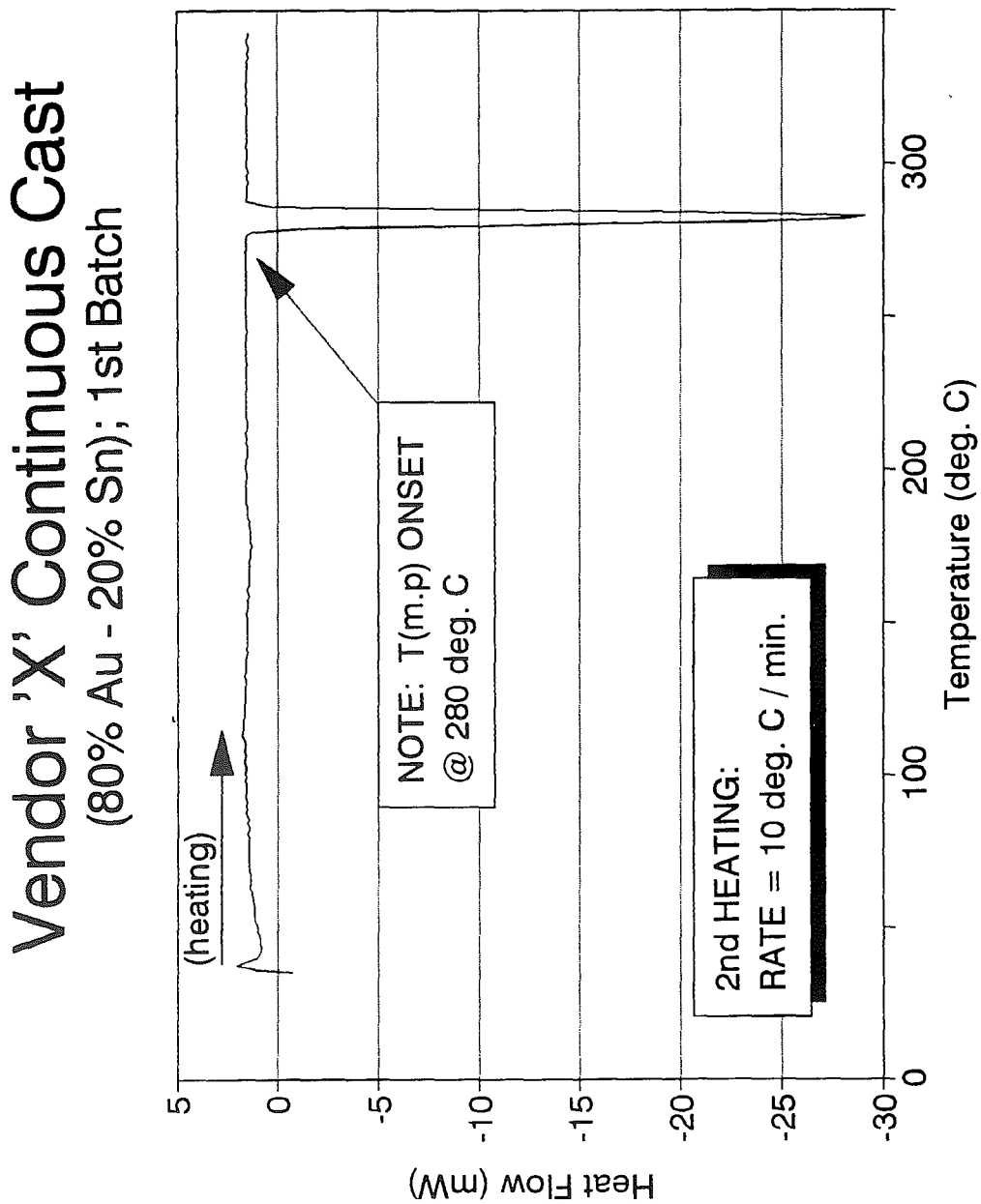

FIGURE 36: DSC Trace for Vendor 'X' -- Continuous Cast (80% Au - 20% Sn). Batch #1 -- 2nd Heating at 10° C / min. from 35° C to 350° C.

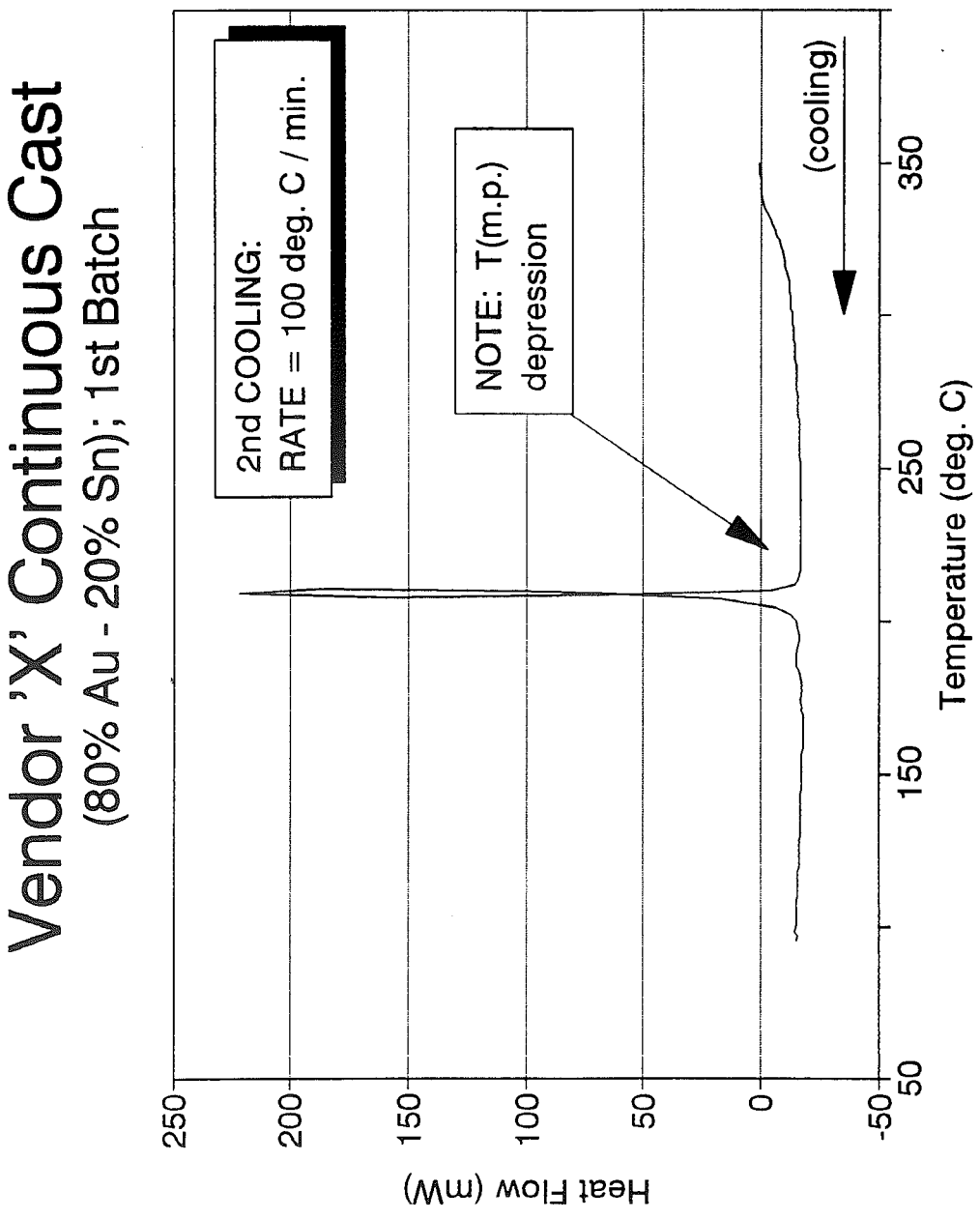

FIGURE 37: DSC Trace for Vendor 'X' -- Continuous Cast (80% Au - 20% Sn). Batch #1 -- 2nd Cooling at 100° C / min. from 350° C to 35° C.

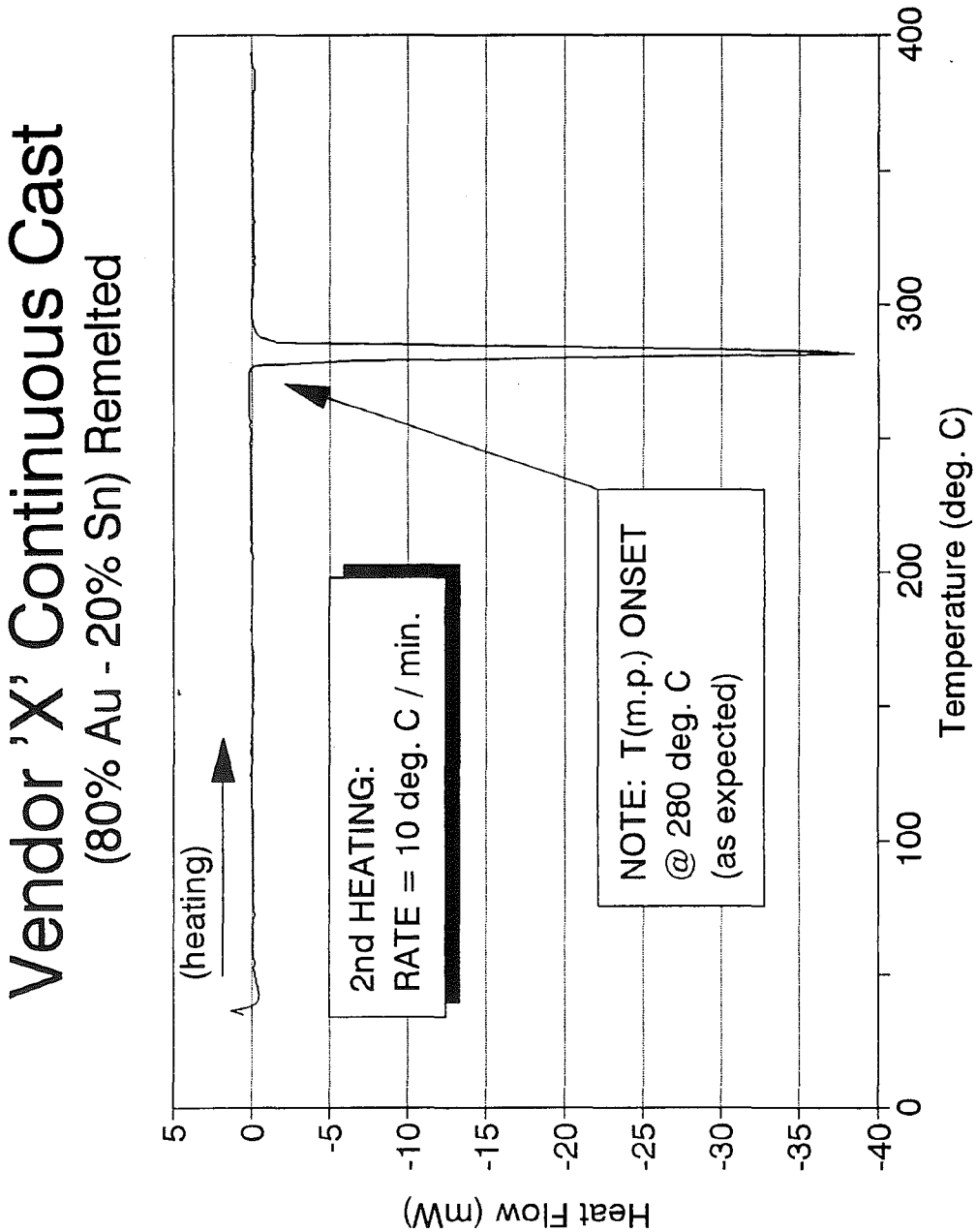

FIGURE 38: DSC Trace for Vendor 'X' -- Continuous Cast (80% Au - 20% Sn) Remelted -- 2nd Heating at 10° C / min. from 35° C to 400° C

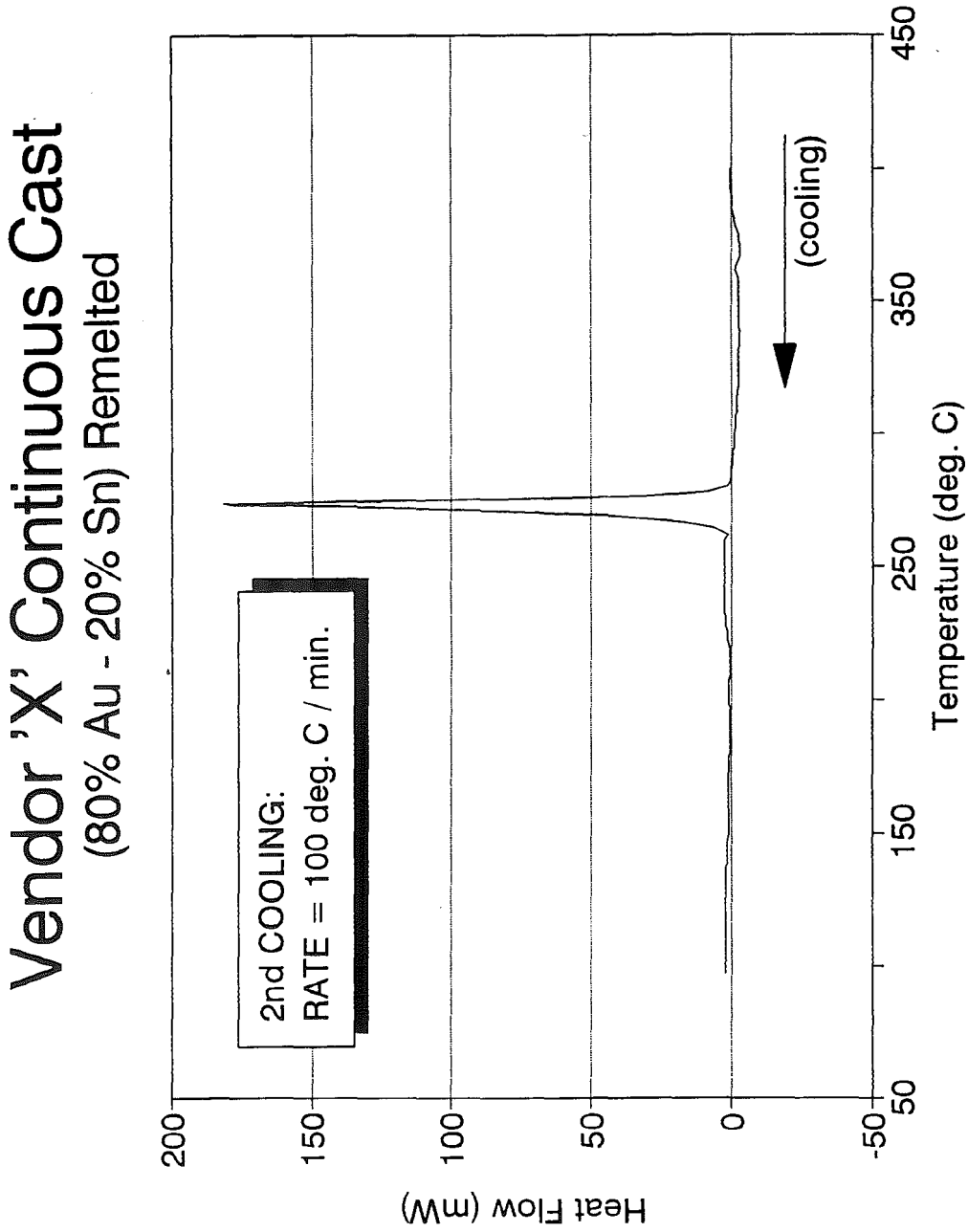

FIGURE 39: DSC Trace for Vendor 'X' -- Continuous Cast (80% Au - 20% Sn) Remelted -- 2nd Cooling at 100° C / min. from 400° C to 35° C.

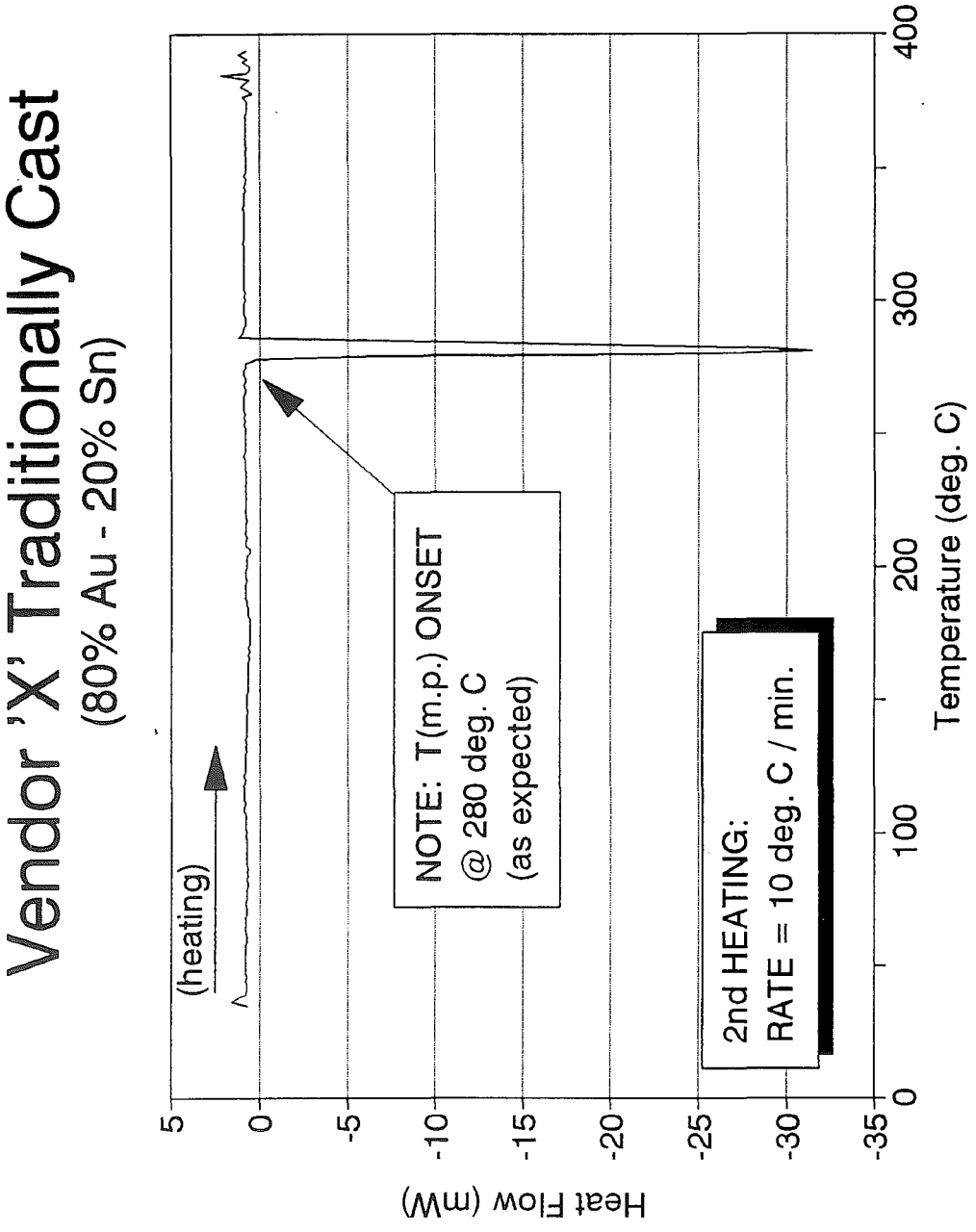

FIGURE 40: DSC Trace for Vendor 'X' -- Traditional Cast (80% Au - 20% Sn). 2nd Heating at 10° C / min. from 35° C to 400° C.

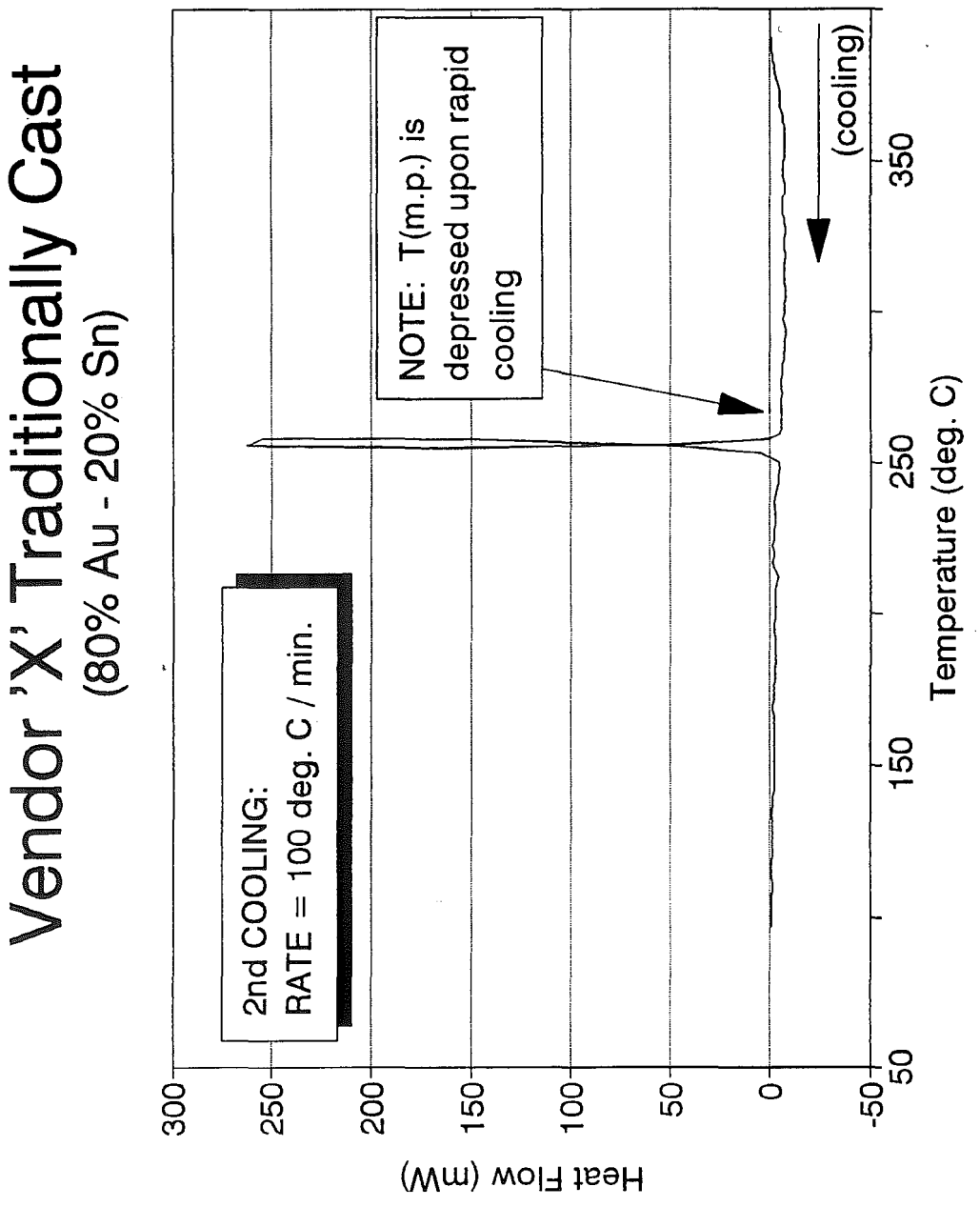

FIGURE 41: DSC Trace for Vendor 'X' -- Traditional Cast (80% Au - 20% Sn). 2nd Cooling at 100° C / min. from 400° C to 35° C.

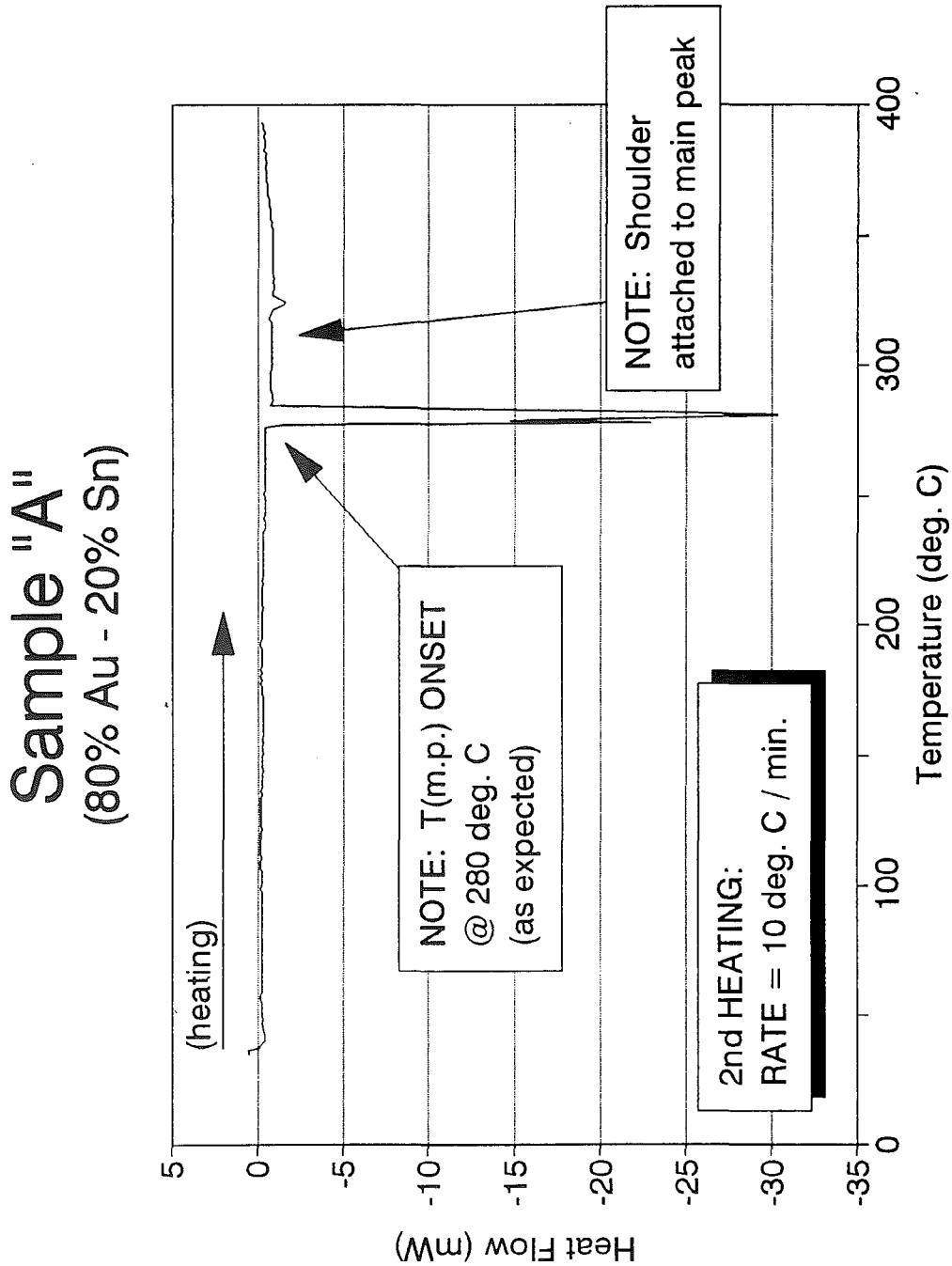

FIGURE 42: DSC Trace for Sample "A" (80% Au - 20% Sn).
2nd Heating at 10° C / min. from 35° C to 400° C.

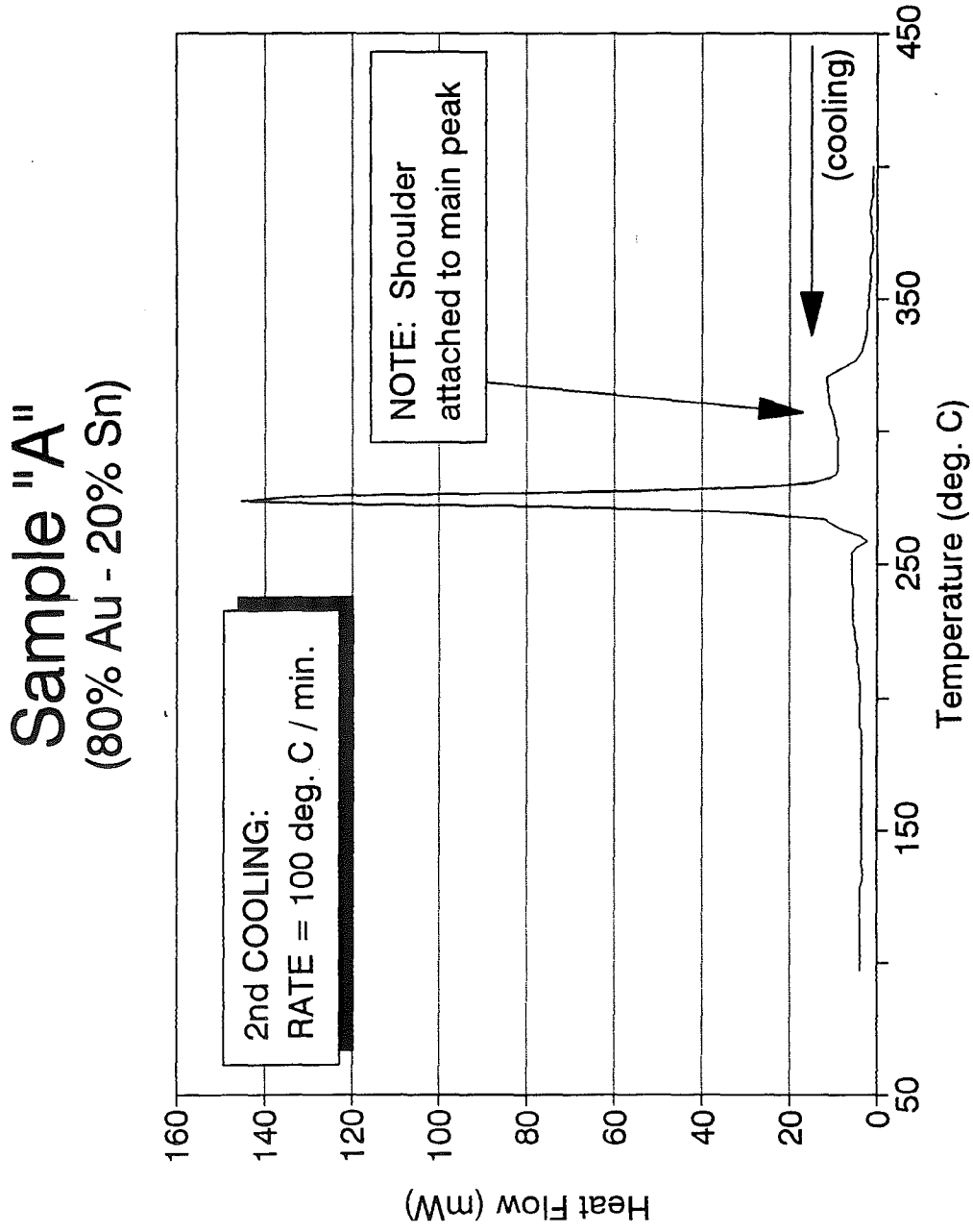

FIGURE 43: DSC Trace for Sample "A" (80% Au - 20% Sn).
2nd Cooling at 100° C / min. from 400° C to 35° C.

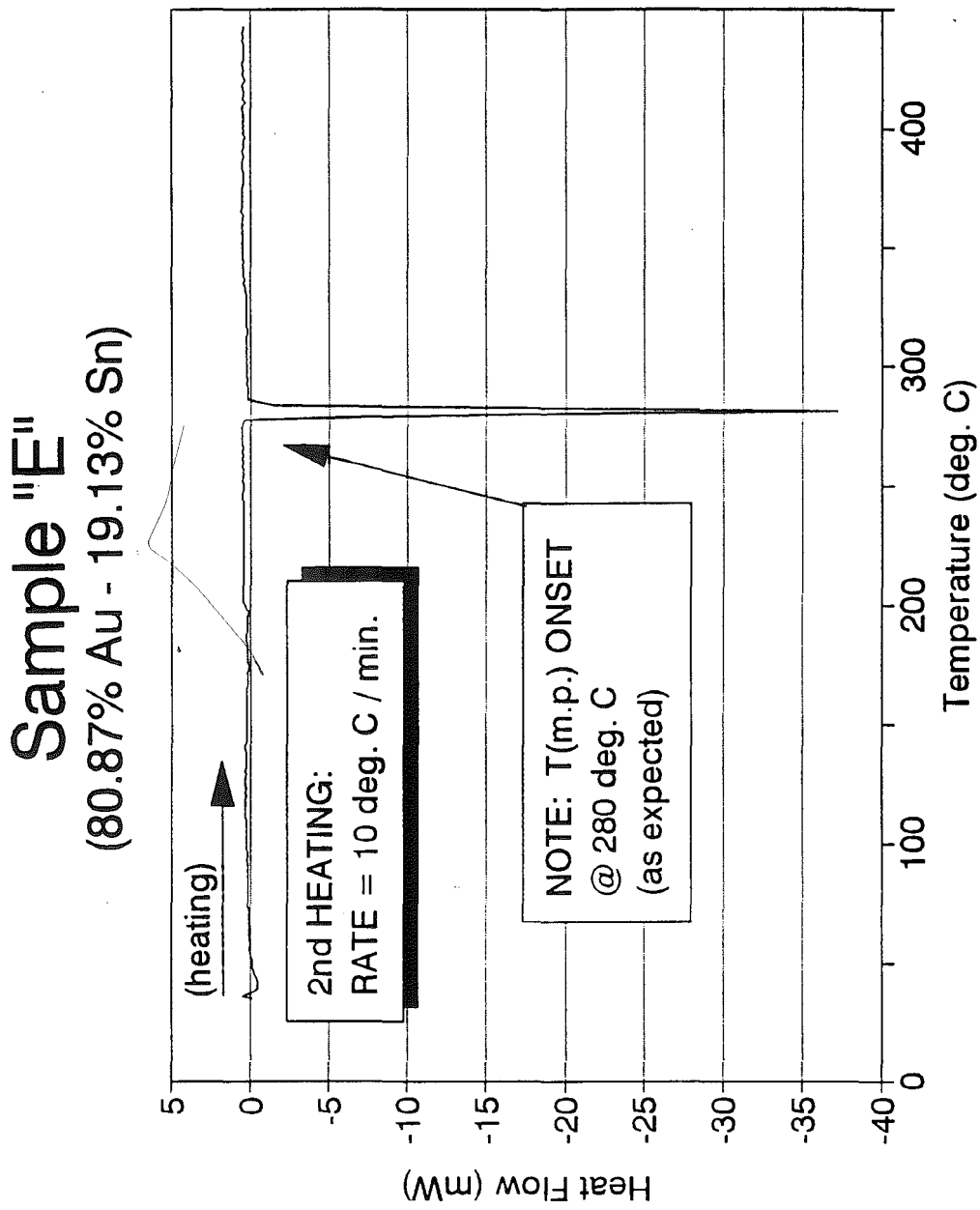

FIGURE 44: DSC Trace for Sample "E" (80.87% Au - 19.13% Sn). 2nd Heating at 10° C / min. from 35° C to 450° C.

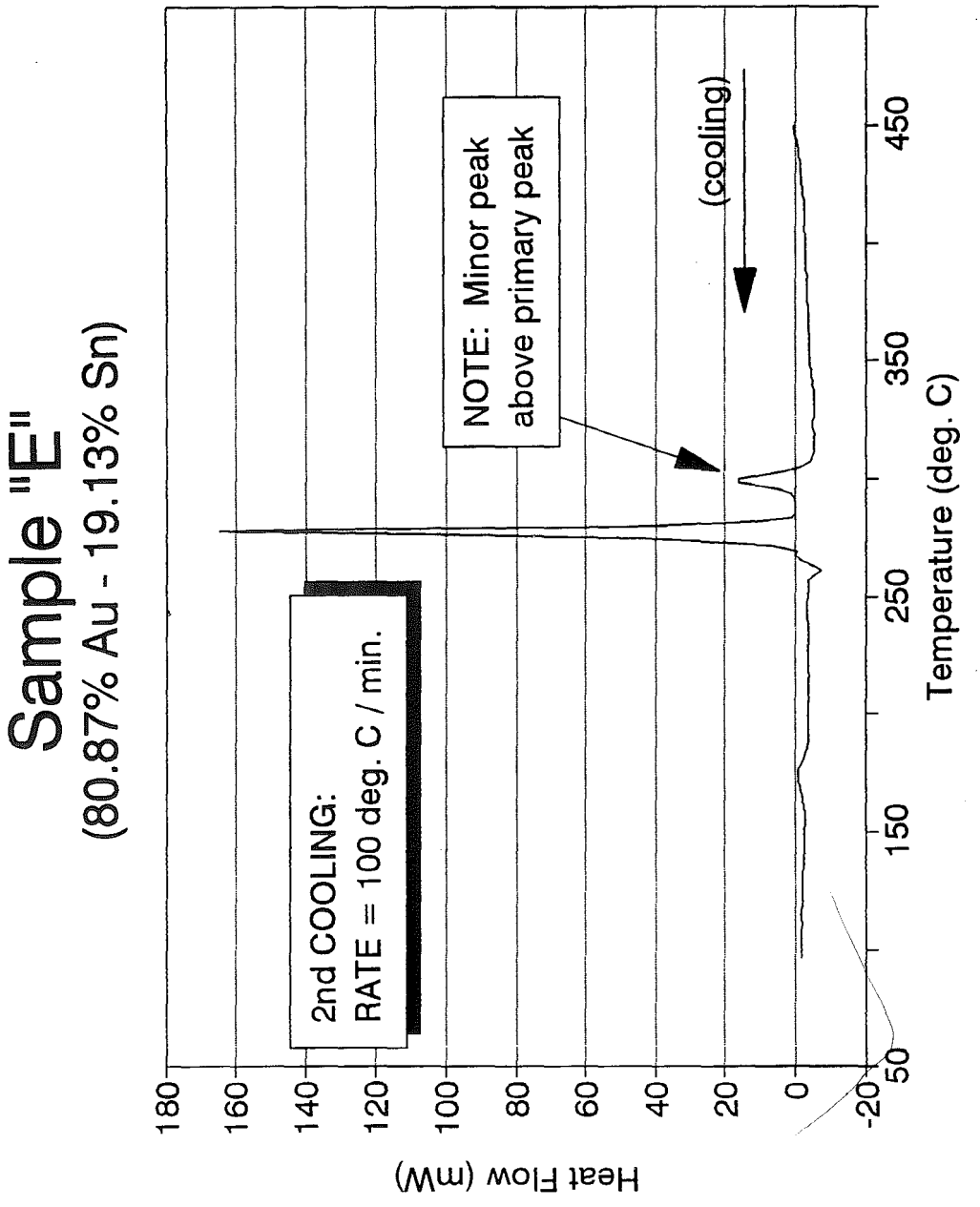

FIGURE 45: DSC Trace for Sample "E" (80.87% Au - 19.13% Sn). 2nd Cooling at 100° C / min. from 450° C to 35° C.

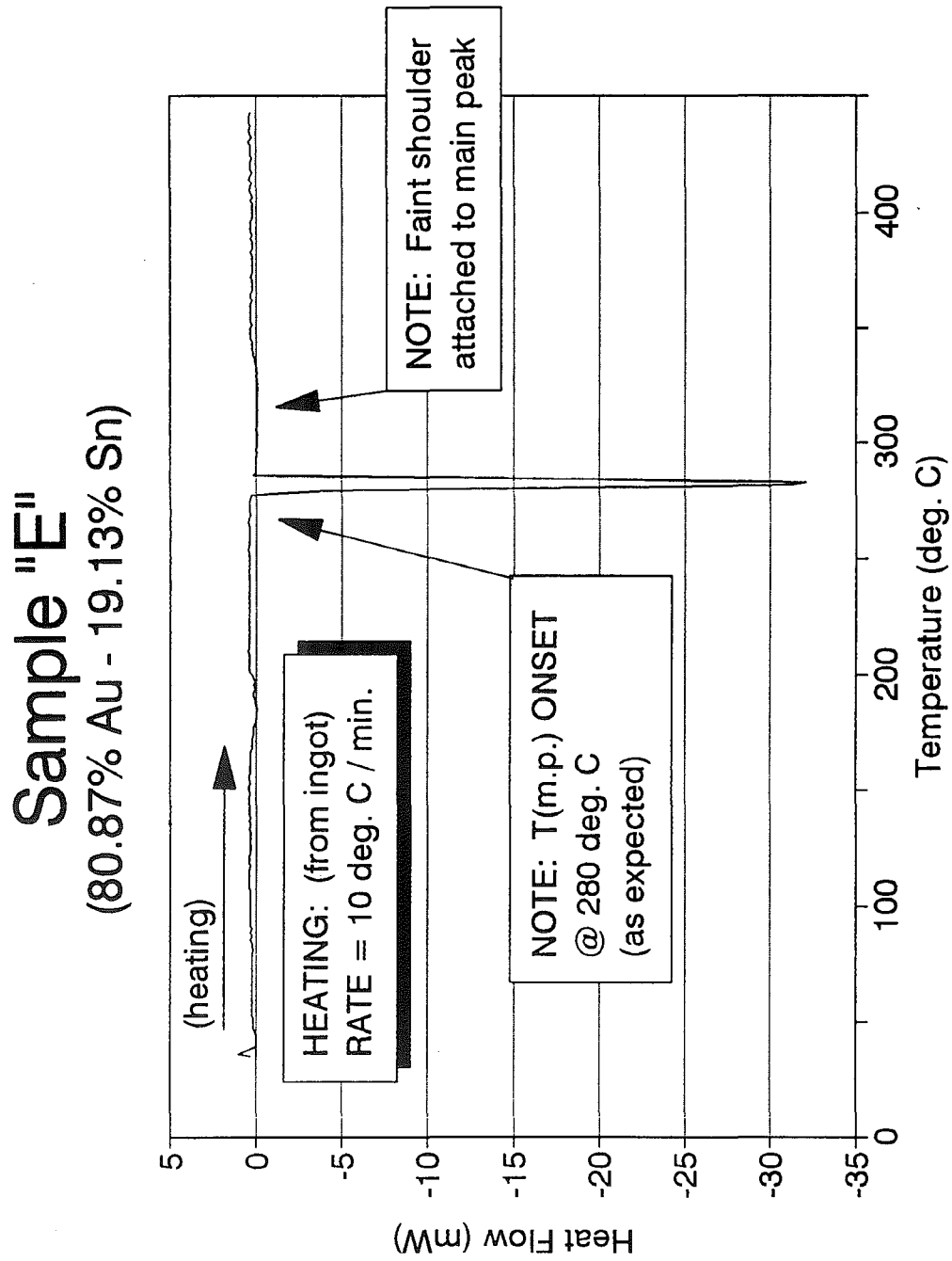

FIGURE 46: DSC Trace for Sample "E" (80.87% Au - 19.13% Sn). 1st Heating (from ingot) at 10° C / min. from 35° C to 450° C.

G. Equilibrium Freezing & Undercooling Effects in Au-Sn Alloys:

The attached schematic (Figure 47) indicates the typical behavior observed for an off-eutectic alloy composition upon cycling through the solid + liquid region of the phase diagram. As the temperature is increased during heating, melting is first observed at the eutectic melting temperature (T_e) as that portion of the microstructure undergoes melting. After the eutectic portion melts and as temperature continues to be increased, the remaining primary phase continues to absorb heat as it melts, the final portion of this solid phase disappearing at the liquidus temperature (T_L). If the specimen is then rapidly cooled to low temperatures, a point will be reached (T_n)where one of the eutectic phases or both is able to nucleate and grow. If cooled directly from the liquid, this supercooling effect can be quite large. If this same alloy is reheated, even though the non-equilibrium solidified product may be locally far from its equilibrium composition, remelting is still not observed until the equilibrium eutectic temperature is reached. This may be explained by the observation that diffusion rates increase rapidly as temperature is increased, and is also much greater in the liquid than the solid. If local melting below (T_e) occurs, diffusion takes place such that the average composition approaches the eutectic composition and refreezes as long as the actual temperature is below (T_e). The net heat change for the two processes is near-zero, and these localized interactions are too low in energy to be recognized by the DSC. At (T_e), any portion of the material that is now at the equilibrium eutectic composition melts, and quickly allows the system to adjust to equilibrium. If the specimen were heated only slightly above the eutectic temperature it would consist mostly of liquid near the eutectic composition and the solid primary β

phase. If the same alloy is now rapidly cooled from the (primary β-plus-liquid) region the undercooling will be smaller than before (now at T_{het}) because nucleation is induced by the presence of the preexisting β phase (schematic, Figure 47).

In the Au-Sn system (Table 5), the values for T_e upon second heating give good agreement with equilibrium melting in all cases. There is a general trend to increase undercooling of the eutectic as the eutectic composition is approached from both sides. The undercooling of the primary phase increases as the alloy becomes more Au-rich or Sn-rich on either side of the eutectic. Both trends are consistent with the above discussion and the description of coupled vs dendritic growth in the following section. Yost, et. al. [27] indicate that the structure of a carefully prepared Au-Sn eutectic alloy (with about the same sample weight as used in this study, viz.,~ 20 g) consisted of (ζ) dendrites in an eutectic matrix, with ~ 46.3 vol. % (δ). Their observation of a dendrite-plus -eutectic structure for an eutectic alloy is consistent with the structure seen in the present study, although Yost, et. al. [27] explain their microstructure as probably being due to a slightly off-eutectic composition. The phase diagram prediction for the volume percent (δ) phase in an eutectic alloy is 44.2 volume percent, and so the volume for (δ) reported by Yost, et. al., would be consistent with a slightly gold-rich alloy. The DSC results for the "eutectic alloy" (80+ wt.% Au) of the present study shows a small thermal arrest at about 320 °C, which is attributed to the gold-rich (ζ) liquidus.

H. Eutectic Solidification vs. Dendritic Growth:

As in the case for pure elements, when an alloy of eutectic composition either melts

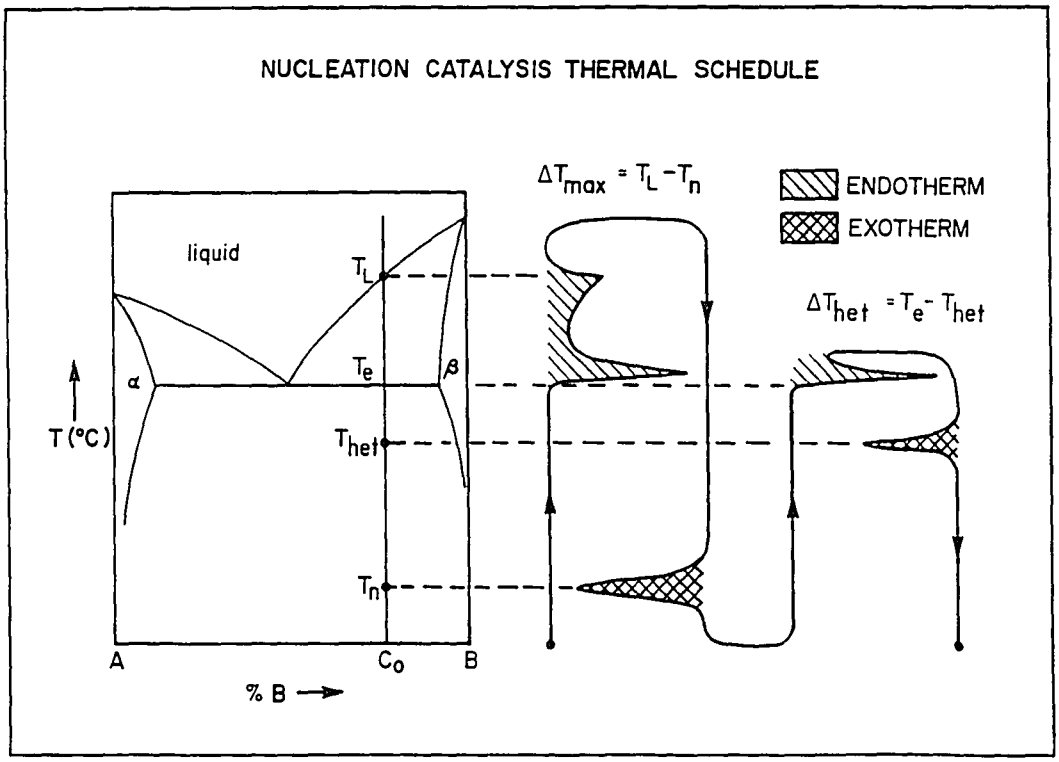

FIGURE 47: Interrupted Thermal Cycling [28]

or solidifies one might expect that there should only be one peak observed in the DSC trace, a peak corresponding to the eutectic melting or freezing temperature. However, because the eutectic temperature may be depressed upon cooling (due to the undercooling of tin-based alloys, as discussed in the previous section) either primary (δ) phase or primary (ζ') phase might be able to nucleate separately rather than as the coupled eutectic structure. The shape of the coupled zone could be related to a difference in the ease of nucleation on each side of the eutectic composition. Tiller [29] has proposed that changes in curvature-free energy and molecular attachment kinetics with temperature (undercooling) can cause the effective eutectic composition to shift (Figure 48). Mueller, et. al., [30] have shown results for the Pb-Sb system which may be interpreted as demonstrating such behavior (Figure 49). Kurz and Fisher [31] have demonstrated that a widened region of coupled eutectic growth appears at both a.) low growth rates in the presence of high temperature gradients, and b.) at high growth rates in the presence of large undercoolings. These same authors show that symmetrical coupled zones are found for regular (non-faceted / non-faceted) eutectics (Figure 50a), and this reflects the similar undercoolings of the two primary dendrite type-phases. A skewed zone tends to occur in an irregular (faceted / non-faceted) eutectic (Figure 50b) because of the high undercoolings attainable for the eutectic and the faceted primary phase, compared to the smaller undercooling attainable in the non-faceted phase. Thus the skewed coupled zone tilts away from the non-faceted phase (towards the faceted phase). It is therefore possible that a completely eutectic microstructure may not be obtained when an alloy having the eutectic composition is solidified rapidly. Kurz & Fisher point out that because the

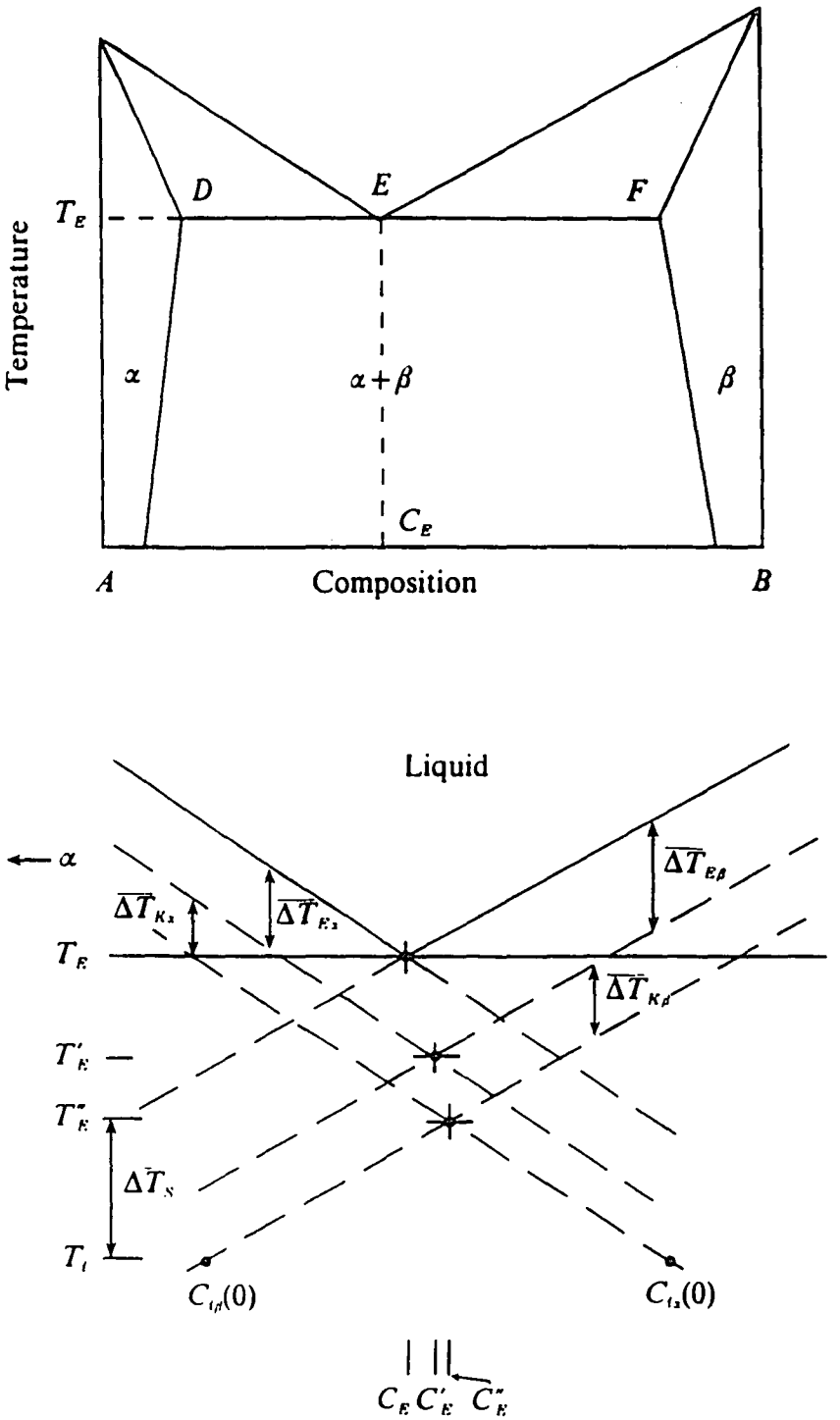

FIGURE 48: Effective Shift of the Eutectic Composition [29]

Summary of undercooling behavior in Pb-Sb alloys. Different symbols refer to undercooling trends produced by different droplet surface coating treatments.

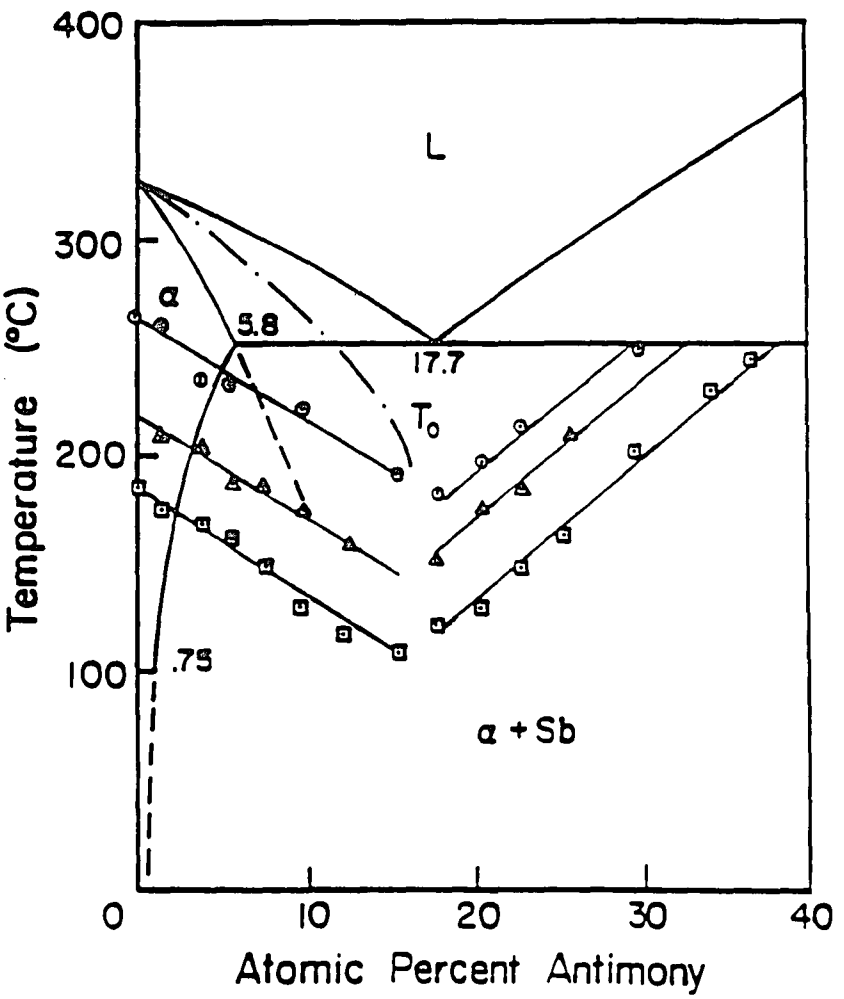

FIGURE 49: Summary of Undercooling Behavior in Pb-Sb alloys [30]

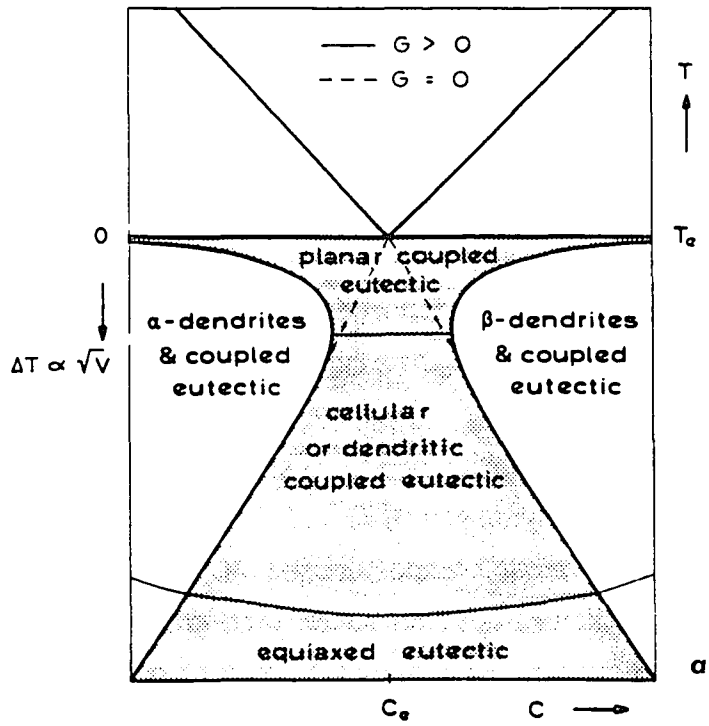

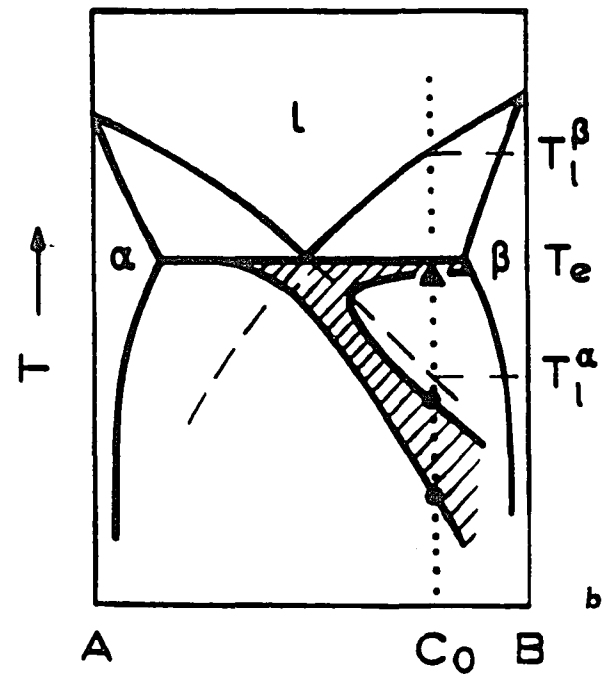

FIGURE 50: a.) Symmetrical Coupled Growth Zone exhibited in regular (non-faceted / non-faceted) eutectics [31].

b.) Skewed Coupled Growth Zone exhibited in irregular (faceted / non-faceted) eutectics [31].

coupled zone is skewed towards the faceted phase, a composition slightly richer in the faceted element must be used to obtain eutectic structures free of dendrites. It is believed that this is the case for the eutectic on the gold-rich side of the Au-Sn system. Microstructures of the primary (δ) phase often appear faceted (Figure 51) while the (ζ) dendrites on the gold rich side of the eutectic appear non-faceted. Coupled growth is therefore easier to achieve on the Sn-rich side of the eutectic, and the appearance of excess (δ) phase is suppressed. On the gold-rich side, however, only small undercoolings are needed to cause the growth of the (ζ) phase dendrite. If the alloy composition is already on the gold rich side of the eutectic, the (ζ) primary phase nucleated above the eutectic can act as heterogeneous nucleation sites for the continued growth of this phase. This could appear as a higher then predicted volume fraction of (ζ) phase dendrites for gold-rich alloys.

The observed agreement between calculated and measured volume percent primary (δ) phase for tin-rich alloys, versus the larger than expected amount of primary (ζ or ζ') phase for gold-rich alloys can therefore be explained in terms of the skewed shape of the coupled zone for the Au-Sn system, and the ease of nucleation of (ζ) phase at small undercoolings.

Finally, as pointed out by Kurz and Fisher [31], at very rapid cooling rates or very high undercoolings, it might even be possible to nucleate the non-faceted dendrite-phase on the opposite side of the equilibrium eutectic composition. Thus, it might be interesting to very rapidly cool eutectic or slightly Sn-rich alloys and examine the microstructures to see if (ζ) phase dendrites form.

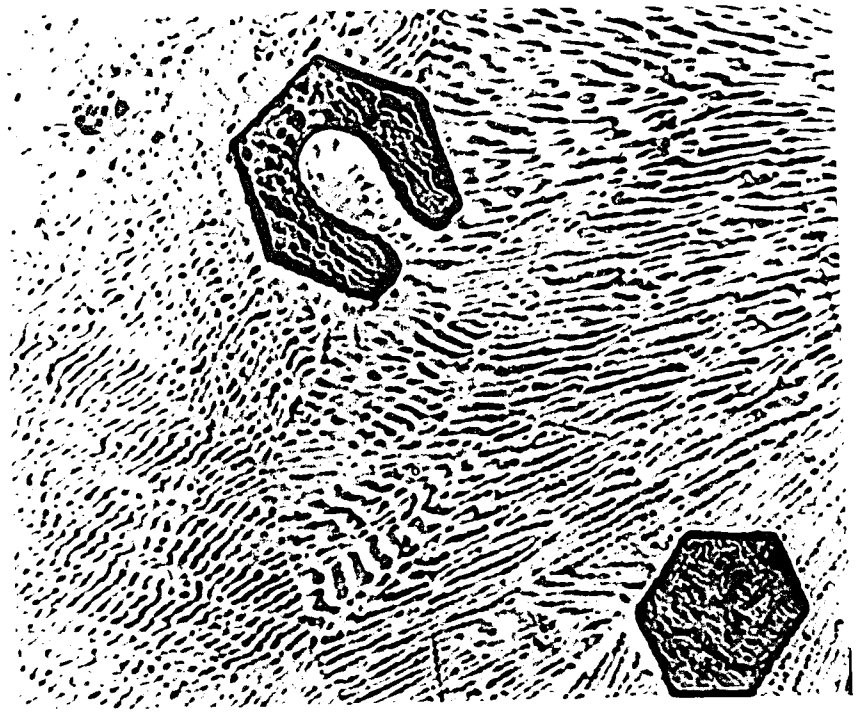

FIGURE 51: a.) Vendor 'X' Continuous Cast (80 wt.% Au - 20 wt.% Sn) Remelted Alloy. Primary (δ) phase (dark, hexagonal) surrounded by eutectic. Light optical microscopy (1600X).

A model for quantitative metallography was developed to calculate area (volume) fraction of dendrite phase in a eutectic two-phase matrix. The model was applied to Au-Sn eutectic alloy and near-eutectic alloy compositions, and was shown to give good agreement with predictions from the phase diagram for eutectic and tin-rich compositions. Alloys on the gold rich side of the eutectic composition give structures showing primary (ζ or ζ') phase dendrites plus eutectic. The volume fraction of dendrites observed for these alloys is consistently greater than predicted and is attributed to easy heterogeneous nucleation of this phase with undercooling. Alloys on the tin rich side of the eutectic composition give structures showing primary (δ) phase, plus eutectic, in excellent quantitative agreement with the model calculations. Alloys at the eutectic composition may show 100 % eutectic structures or eutectic plus dendrites depending on the cooling conditions. DSC results on the gold rich side of the eutectic composition indicate two thermal arrests; one corresponds to the eutectic transformation and the other corresponds to the primary (ζ) phase liquidus. DSC results on the tin rich side of the eutectic composition likewise indicate two thermal arrests; one corresponds to the eutectic and the other corresponds to the primary (δ) phase liquidus. For both gold-rich and tin-rich alloys, the measured liquidus values agree well with the values predicted from the phase diagram. Alloys at the eutectic composition show only one peak corresponding to the eutectic transformation. For all alloy compositions a DSC peak for the peritectoid (at ~ 190 °C) is observed upon reheating supercooled alloys.

References

1. Charles L. Hutchins, "Solder Reflow for SMT," Proceedings of 2nd ASM International Electronic Materials and Processing Congress, Philadelphia, PA, (1989) 433.

2. Ken'ichi Mizuishi, Masahide Tokuda, Yuuji Fujita, "Fluxless and Virtually Voidless Soldering for Semiconductor Chips." *IEEE Transactions on Components, Hybrids, and Manufacturing Technology,* 11 (4), (1988) 447.

3. Goran S. Matijasevic, Chin C. Lee and Chen Y. Wang, "Extremely Reliable Bonding of Large Silicon Dice Using Gold-Tin Alloy," Proceedings of 40th IEEE Electronic Components and Technology Conference, New York, (1990) 786.

4. Gordon J. Davy, "Inspection - Key to Soldering Process Development and Control," Proceedings of 2nd ASM International Electronic Materials and Processing Congress, Philadelphia, PA, (1989) 443.

5. Michael Santella, "Fundamental Metallurgical Considerations in Brazing and Soldering," Proceedings of the Metal Science of Joining, Cincinatti, OH, (1991) 62.

6. J. Ciulik and M. R. Notis, "The Au-Sn Phase Diagram," *Journal of Alloys and Compounds (formerly the Journal of Less-Common Metals),* 191 (1), (1993) 71.

7. Paul O. Johnson and Mike Wolverton, "A Solderability Problem's Cause is Determined for Gold -Tin Preforms in Mulitchip Modules," *The International Journal for Hybrid Microelectronics,* 14 (3), (1991) 96.

8. R. J. Wassink, Soldering in Electronics Second Edition, Electrochemical Publications, Ltd., England, 1989, 472.

9. P. S. Mohanty, F. H. Samuel, and J. E. Gruzleski, "Mechanisms of Heterogeneous Nucleation of Pores in Metals and Alloys," *Metallurgical Transactions A,* 24A (8), (1993) 1845.

10. Chin C. Lee, Chen Y. Wang and Goran S. Matijasevic, "A New Bonding Technology Using Gold and Tin Multilayer Composite Structures," *IEEE Transactions on Components, Hybrids and Manufacturing Technology,* 14 (2), (1991) 407.

11. Masanori Nishiguchi, Noboru Goto and Hideaki Nishizawa, "Highly Reliable Au-Sn Eutectic Bonding with Background GaSi LSI Chips." *IEEE Transactions on Components, Hybrids and Manufacturing Technology,* 14 (3), (1991) 523.

12. Mettler TA 3000 Operating Manual.

13. V. J. Kuck, "Determination of the Liquidus Temperature and Composition of Tin/Lead Solders Using Differential Thermal Analysis," *Thermochemica Acta,* 99 (1986) 233.

14. B. D. Cullity, Elements of X-Ray Diffraction 2nd Edition, Addison-Wesley Publishing Company, Inc., Reading, MA, 1978, 87.

15. J. Ciulick, "An Experimental Determination of the Gold-Rich Portion of the Gold-Tin Phase Diagram," Masters Thesis, Department of Materials Science and Engineering, Lehigh University, (1988).

16 J. I. Goldstein, D. E. Newbury, P. Echlin, D. C. Joy, A. D. Romig, C. E. Lyman, C. Fiori, E. Lifshin, Scanning Electron Microscopy and X-Ray Microanalysis, Plenum Press, New York, 174.

17. E. E. Underwood, Quantitative Stereology, Addison-Wesley Publishing Company, Inc., Reading, MA, 1970.

18. John C. Russ, Computer-Assisted Microscopy The Measurement and Analysis of Images, Plenum Press, New York, 1990.

19. R. T. DeHoff and F. H. Rhines, Quantitative Microscopy, McGraw-Hill, New York, 1968.

20. John C. Russ, Practical Stereology, Plenum Press, New York, [ISBN 0-306-42460-6].

21. William F. Smith, Principles of Materials Science and Engineering, McGraw-Hill Book Company, Inc., New York, 1986.

22. R. Roche, "The Use of the 'Quantimet' Microscope in the Micrographic Quantitative Determination of Combined Oxygen at Oxide Inclusions," *The Microscope,* 16 (2), (1968) 151.

23. Delesse, (1848), *Procede mecanique pour la determination de la composition des roches. Annales des Mines, 13 4eme serie 379.*

24. Z. Paley and M. W. Williams, "The Quantitative Estimation of Phases in Cast Irons," International Conference on Quantitative Relations Between Properties and Microstructure, D. G. Brandon and A. Rosen, editors, (1969).

25. G. Humpston and D. Jacobson, Principles of Soldering and Brazing, ASM International, Materials Park, OH, (1993) 57.

26. IBM Unpublished Work, with the permission of the investigator, Vince Marcotte, (1983).

27. F. G. Yost, M. M. Karnowsky, W. D. Drotning, and J. H. Gieske, "Thermal Expansion and Elastic Properties of High Gold-Tin Alloys," *Metallurgical Transactins A*, 21A (7), (1990) 1885.

28. J. H. Perepezko, "Thermal Analysis of Solidification Kinetics," Thermal Analysis in Metallurgy, D. Shull and A. Joshi, eds., TMS, (1990) 121.

29. W. A. Tiller, The Science of Crystallization: Macroscopic Phenomena and Defect Generation, Cambridge University Press, (1991) 309.

30. B. A. Mueller, J. J. Richmond, and J. H. Perepezko, "Solidification Structures Developed in Al-Si and Pb-Sb Alloys," Rapidly Quenched Metals, S Steeb, and H. Warlimont, eds., Elsevier, (1985) 47.

31. W. Kurz and D. J. Fisher, Fundamentals of Solidification, Trans Tech, (1989) 109.

Edward Laurence Martin, son of Dr. Edward C. Martin, and Marion B. Martin was born June 5, 1969 in Plainfield, New Jersey. He graduated from Westfield Senior High School, Westfield, New Jersey, with honors, in June, 1987. He attended Lehigh University, Bethlehem, Pennsylvania and received a B.S. in Materials Science and Engineering in January, 1992. Following the advice of his father and his advisor he continued his study of Materials Science and Engineering by commencing graduate studies at Lehigh University the day after his undergraduate graduation. Two years later this thesis became a reality. Upon completion of graduate studies Edward will begin his professional career with Texas Instruments, Inc., Attleboro, MA. However, he hopes one day to return to the world of higher education to obtain his doctorate.

END

OF

TITLE